AIMS Materials Science, 4(3): 755-788.
DOI: 10.3934/matersci.2017.3.755
Received: 30 April 2017
Accepted: 08 June 2017
Published: 14 June 2017

http://www.aimspress.com/journal/Materials

Review

Characterization techniques for graphene-based materials in catalysis

Maocong Hu, Zhenhua Yao, and Xianqin Wang *

Department of Chemical, Biological and Pharmaceutical Engineering, New Jersey Institute of Technology, Newark, NJ 07102, USA

* **Correspondence:** Email: xianqin.wang@njit.edu; Tel: +1-973-596-5707; Fax: +1-973-596-8436.

Abstract: Graphene-based materials have been studied in a wide range of applications including catalysis due to the outstanding electronic, thermal, and mechanical properties. The unprecedented features of graphene-based catalysts, which are believed to be responsible for their superior performance, have been characterized by many techniques. In this article, we comprehensively summarized the characterization methods covering bulk and surface structure analysis, chemisorption ability determination, and reaction mechanism investigation. We reviewed the advantages/disadvantages of different techniques including Raman spectroscopy, X-ray photoelectron spectroscopy (XPS), Fourier transform infrared spectroscopy (FTIR) and Diffuse Reflectance Fourier Transform Infrared Spectroscopy (DRIFTS), X-Ray diffraction (XRD), X-ray absorption near edge structure (XANES) and X-ray absorption fine structure (XAFS), atomic force microscopy (AFM), scanning electron microscopy (SEM), transmission electron microscopy (TEM), high-resolution transmission electron microscopy (HRTEM), ultraviolet-visible spectroscopy (UV-vis), X-ray fluorescence (XRF), inductively coupled plasma mass spectrometry (ICP), thermogravimetric analysis (TGA), Brunauer–Emmett–Teller (BET), and scanning tunneling microscopy (STM). The application of temperature-programmed reduction (TPR), CO chemisorption, and NH_3/CO_2-temperature-programmed desorption (TPD) was also briefly introduced. Finally, we discussed the challenges and provided possible suggestions on choosing characterization techniques. This review provides key information to catalysis community to adopt suitable characterization techniques for their research.

Keywords: graphene; catalysis; characterization; bulk and surface structure; chemisorption ability; reaction mechanism

Nomenclature

G	graphene	FLG	few-layer graphene
GO	graphene oxide	NG	nitrogen doped graphene
rGO	reduced graphene oxide	HER	Hydrogen evolution reaction
SLG	single-layer graphene	SAED	selected area electron diffraction
QHE	the quantum hall effect	DFT	Density Functional Theory computations
CVD	chemical vapor deposition	XPS	X-ray photoelectron spectroscopy
ORR	oxygen reduction reaction	HR-TEM	high-resolution transmission microscopy
OER	oxygen evolution reaction	FTIR	Fourier transform infrared spectroscopy
XRF	X-ray fluorescence	N-GQDs	nitrogen-doped graphene quantum dots
TGA	thermogravimetric analysis	TPR	temperature-programmed reduction
MS	Mass spectrometry	TPD	temperature-programmed desorption
XRD	X-ray diffraction	STM	scanning tunneling microscopy
AFM	atomic force microscope		

1. Introduction

Graphene (G), the amazing two-dimensional carbon allotrope [1], has attracted great attention from both the scientific and engineering communities in last decade since its discovery in 2004 [2,3,4]. It is a single-layer hexagonal lattice made of carbon atoms in a sp^2 hybridized configuration, which is the basic structural element of other carbon allotropes including graphite, carbon nanotubes and fullerenes [5]. Based on the number of layers, graphene can be categorized roughly into monolayer, few-layer, and multi-layer ones. The unique structure allows it to have many unusual and attractive properties such as quantum hall effect (QHE), large surface area, superior intrinsic electron mobility, and excellent thermal conductivity. These superior properties make it and its derivatives as versatile materials in a wide range of areas including separation [6], environmental protection [7], memory devices [8,9], energy [10,11,12], optical instruments [13], sensor [14], medicine [15], and catalysis [16,17].

Numerous catalytic reactions have been attempted over graphene-based catalysts such as oxygen reduction [18], selective hydrogenation [19], NO_x abatement [20], air purification [21], and waste water treatment [22], while many promising and exciting results were achieved. Especially, due to its superior intrinsic electron mobility, high surface area, transparency, locally conjugated aromatic system, and high chemical and electrochemical stability, graphene has been widely used in photocatalytic applications [23–31]. The advantage of graphene-based materials in catalysis is believed to be related to their large specific surface area, two-dimensional structure, excellent electrical and thermal conductivity, high mechanical strength, high adsorption capacity for certain molecules, and easiness of modification, which were characterized by many techniques [32]. Although many review articles were presented about graphene-based materials in catalysis, the highlights were usually focused on reporting superior reaction performance or summarizing synthesis methods while the characterization techniques were simply mentioned in a very limited part of their whole texts or integrated in the above two parts [33,34]. There are also several review papers

published focusing on individual techniques such as XPS [35] and Raman [36,37] to characterize graphene and graphene-related compounds used in many fields such as semiconductor, biomedical, and physical applications. However, to our best knowledge, thus far there is no separate article to comprehensively discuss the development and advance of the characterization techniques for graphene-based materials in catalysis. In this article, we reviewed the main characterization approaches covering bulk and surface structure analysis, chemisorption ability determination, and reaction mechanism investigation in this field (Figure 1). It covered all aspects on characterizing graphene-based materials in catalytic research. We also discussed the challenges and suggestions on choosing characterization techniques. This review provides key information to catalysis community to adopt suitable characterization techniques for their research.

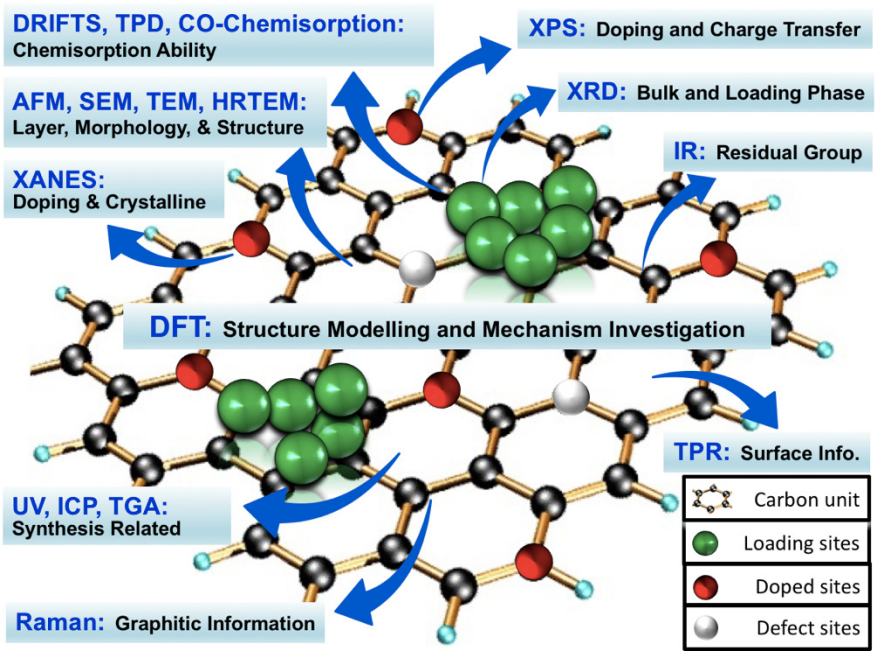

Figure 1. Schematic diagram of characterization techniques for graphene-based materials in catalysis.

2. Bulk and Surface Structure Analysis

Due to the unique bulk and surface structure, the characterization techniques employed for graphene-based materials are different from traditional catalysts. The most powerful approaches include Raman spectroscopy, X-ray photoelectron spectroscopy (XPS), Fourier transform infrared spectroscopy (FTIR), X-Ray diffraction (XRD), X-ray absorption near edge structure (XANES) and X-ray absorption fine structure (XAFS), atomic force microscopy (AFM), scanning electron microscopy (SEM), transmission electron microscopy (TEM), high-resolution transmission electron microscopy (HRTEM), ultraviolet-visible spectroscopy (UV-vis), X-ray fluorescence (XRF), inductively coupled plasma mass spectrometry (ICP), thermogravimetric analysis (TGA), Brunauer–Emmett–Teller (BET), and scanning tunneling microscopy (STM). We covered each technique with its fundamental mechanism and specific application in graphene-based catalysis, we also discussed the challenges and key points in the end.

2.1. Raman Spectroscopy

Raman spectroscopy was built based on the well-known Raman Effect involving the absorption (Stokes process) and emission (anti-Stokes process) of phonons, which was first discovered by C. V. Raman and his colleagues in 1928. It's adopted by catalysis community and widely used in many catalytic studies due to its excellent performance for both catalyst structure determination and in situ reaction monitoring [38,39]. Moreover, Raman spectroscopy is one of the best tools to investigate the structure and quality of carbon-based materials including graphene [40,41]. It's a strong, rapid, sensitive and non-destructive analytical approach to provide both qualitative and quantitative information for graphene-based catalysts. The bulk and surface structure of graphene-based catalysts such as functional groups on the surface, chemical modification of graphene matrix, number of layers, and structural damage due to heteroatom doping, were widely investigated in the related study.

Generally, graphene has six normal modes and two atoms per unit cell at the so-called Brillouin zone center (Γ), where (Γ) = A_{2u} + B_{2g} + E_{1u} + E_{2g} [36]. Especially, the E_{2g} phonons are active in Raman spectroscopy. The D peak (at 1320–1350 cm^{-1}), G peak (at 1580–1605 cm^{-1}), and 2D or named G' peak (at 2640–2680 cm^{-1}) are the three predominant features of Raman spectrum for graphene (as shown in Figure 2). The D mode is related to the defect and disorder level within the graphite layers while the G and 2D bands represents the two-dimensional hexagonal lattice. In some cases, the D' peak is also observable at ~1602–1625 cm^{-1} [42,43], which is related to the defect-induced and double-resonance process. The observation of these characteristic peaks can be studied over graphene-based catalysts, while some parameters like line-widths, intensities, and peak position may show little change compared to pristine graphene due to the effects from a number of factors such as catalyst-graphene (support) interaction, number of graphene layers, heteroatom doping, strain, etc. For example, Omidvar et al. [44] prepared graphene oxide (GO)/Pd nanocomposite via immobilizing Pd on the surface of the GO and further applied it for catalytically degrading organic dyes in water. Two characteristic bands (D and G) were observed in Raman spectrum. The D peak (~1335 cm^{-1}) was attributed to the defects and disorder while the G band (~1593 cm^{-1}) was ascribed to the first order scattering of the E_{2g} phonon of sp^2 carbons atoms. Furthermore, the authors calculated the intensity ratio of the both peaks (I_D/I_G), which is usually used to qualitatively compare the density of structural defects. They found the value for the GO (1.55) was higher than that from the GO/Pd catalyst (1.2), which was attributed to the successful reduction of GO in GO/Pd catalyst during the preparation process. Rout et al. [45] used a one-step deposition-precipitation approach to synthesize the high active and well defined reduced graphene oxide (rGO) supported Au–Cu alloy catalysts for multiple reactions. The authors used Raman spectroscopy to analyze the level of modification on the GO surface. Similarly, two main peaks (D and G bands) were observed in the spectrum while the peak position shifted to lower wavenumber over Au_3–Cu_1/rGO catalyst compared to the GO precursor. Moreover, they found that the I_D/I_G ratio of catalyst was higher (1.1) than that of GO (0.94). The authors concluded that a conjugated sp^2 graphene network was re-established based on this increase in I_D/I_G value.

It's important to analyze (qualitatively or quantitatively) the number of layers of graphene in graphene-based catalysts since it would determine the surface area of the catalysts and finally affect the catalytic performance. Usually, a monolayer graphene sheet shows the Lorentzian peak for 2D at 2679 cm^{-1}. However, in practical catalytic applications, multilayer graphene supports are mostly

achieved while the 2D peak would shift toward higher wavenumber and becomes broader. Shahid et al. [46] used this method to differentiate number of layers of the graphene qualitatively over their synthesized and reduced graphene oxide (rGO) supported cobalt oxide catalysts for oxygen reduction. The 2D bands for GO was observed at 2702 cm^{-1}, indicating its multilayer structures. That for rGO was 2694 cm^{-1}, which also suggested the existence multilayer and was attributed to the removal of oxygen functional moieties (of GO) which may prevent the graphene layers from stacking. Interestingly, the rGO@Co_3O_4 catalyst exhibited a 2D peak at 2694 cm^{-1}. The author proposed that Co_3O_4 nanocubes might act as nanospacers to retard restacking of the graphene sheets by intercalating into different graphene layers, which finally facilitated the formation of single or few layer graphene.

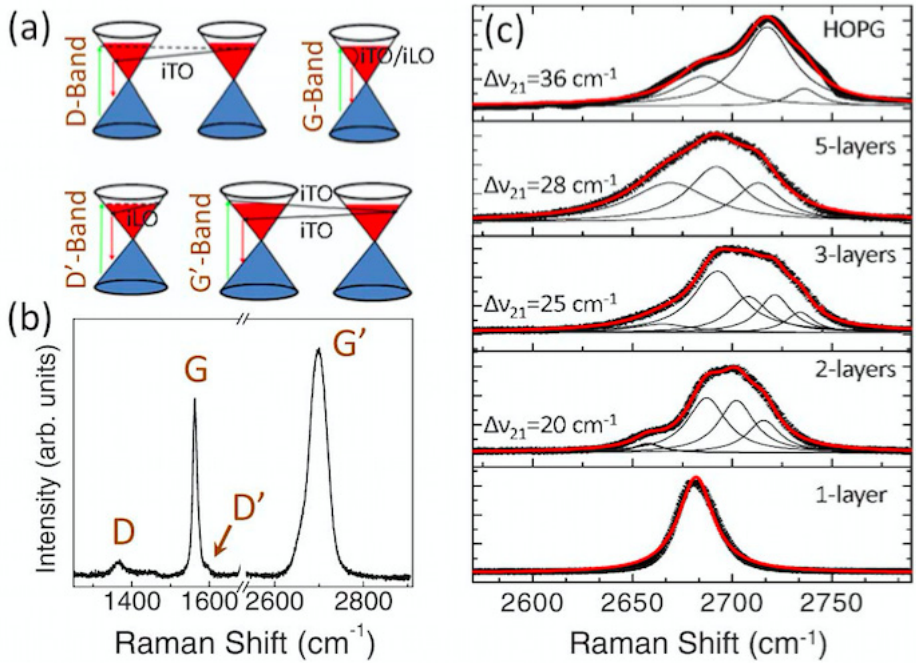

Figure 2. Raman spectroscopy analysis for graphene: scattering mechanism (a), typical spectrum (b), and layers number determination by G' (i.e., 2D) band deconvolution (c) (Reprinted with permission from ref [43]. Copyright 2007, AIP Publishing LLC).

Another approach using 2D band for quantitatively determining layer number was originally proposed by Ferrari et al. [47] and had been widely adopted [43,48,49]. For example, Begliarbekov et al. [43] built a quantitative relationship between Δ_{21} and the number of layers of graphene, where Δ_{21} is the value of difference in wavenumbers of the two dominant subcomponents after curve fitting over 2D band (Figure 2). For a single layer, there is only one highly symmetrical peak ($\Delta_{21} = 0$). For few or multi layers of graphene-based materials, the Δ_{21} would increase with the number of layers. They concluded that the corresponding values for 2, 3, and 5 layers graphene and highly ordered pyrolized graphite (HOPG) were 20, 25, 28, and 36 cm^{-1}. It's worth noting that the Δ_{21} value may have slight difference due to the effect from complex structure after loading different catalytic active species.

Another factor affecting reaction performance of graphene-based catalysts is the in-plane crystallite sizes (L_a) of graphene sheet. For example, in the heteroatom doping graphene catalyst, the

substitution of heteroatoms into graphene matrix usually introduces defects into the graphene surface. The La can be considered as the average distance of the inter-defects, which can be used to investigate defects introduced due to heteroatoms doping. That is, smaller La corresponds to more defects while perfect graphene structure shows huge La value. The La value can also be determined quantitatively by the Raman spectroscopy according to the Tuinstra-Koenig (TK) relation, $L_a(nm) = (2.4 \times 10^{-10})\cdot\lambda^4(I_D/I_G)^{-1}$ (λ is the Raman excitation wavelength, I_D/I_G is the intensity ratio of the D and G band in Raman spectra) [50]. For example, Oh et al. [51] used TK relation to calculate the crystalline domain size of the synthesized graphene (G) and nitrogen containing graphene (N-G) materials, which aimed to prepare polymer electrolyte membrane fuel cells (PEMFC) anodes. They firstly obtained the I_D/I_G ratio for G (0.1) and N-G (0.5) from the Raman spectra. Then the domain size was determined to be 8.8 and 44 nm, respectively. The authors attributed the size decrease of graphene sheet to the substrate coating due to nitrogen species. This approach could be used more widely especially for those graphene materials achieved from graphite oxide exfoliation, while it is rarely reported in literature. As one of the most developed methods to obtain higher yields of graphene-based catalysts, one big issue with graphite oxide exfoliation is the existence of residual defects even after so-call "complete" reduction of graphene. These residual defects would greatly lower the catalytic performance especially in electrocatalysis and photocatalysis due to their severe influence on charge carrier mobility, surface roughness, electrical conductivity, and charge carrier separation. Thus, it's very important to characterize its structural integrity while La value would be a powerful parameter.

Raman spectroscopy is considered as the standard tool to characterize graphene-based catalysts. Almost all published works related to graphene-based catalysis adopted this technique. However, most of the results were focused on detection of the D and G bands or the comparison between D and G bands qualitatively. Deep understandings on the obtained spectra are usually missing especially with the quantitative analysis of I_D/I_G ratio, 2D band deconvolution and layer number determination, graphene crystalline domain size measurement, and defect level estimation with Tuinstra-Koenig relation.

2.2. X-ray Photoelectron Spectroscopy (XPS)

XPS spectra are obtained by measuring the kinetic energy and the number of electrons that escape from material surface (<10 nm) when the material is irradiated with a beam of X-ray. XPS is a surface-sensitive and powerful quantitative spectroscopic technique. It can be used to characterize elemental composition, chemical state, and electronic state of the elements on the surface, which is crucial for catalytic research [52,53]. It was not in the list of major technique for characterizing graphene-based catalysts until the recent emerged application of the heteroatom doping graphene-based materials in catalysis [54,55]. Now XPS is the standard technique to study the doping effect by investigating the distribution of the heteroatom dopants and the bonding between dopants and carbon atoms. The ratios of peak intensity between dopants and C 1s are used to determine the dopant content in these heteroatom-doped graphene catalysts. Though the exact position of the intrinsic graphene C 1s line is challenging to measure due to sample-related issues such as the scarcity of free-standing single-layer graphene, an approximate value of around 284.6 eV is widely adopted. Especially, once heteroatoms are doped into graphene, C 1s peak will change accordingly. Because many graphene-based catalysts are prepared by graphite oxide exfoliation,

where oxidation is the essential step, the O 1s peak at around 532.4 eV is also observed and affected by dopants. For the different dopants, according to the doping type, there are several corresponding characteristic peaks.

The most useful function of XPS spectrum for graphene-based catalysts is to confirm the presence of the foreign atoms on the graphene by XPS survey spectra. For example, Xu et al. [56] synthesized phosphorus-doped porous graphene (P-G) electrocatalyst for triiodide reduction in dye-sensitized solar cell. The authors observed the C 1s peak at 284.8 eV and O 1s peak at 532.1 eV for graphene (G) in XPS spectra. Two minor peaks P 2s (at 189.1 eV) and P 2p (at 131.1 eV) were detected over P-G. The P doping ratio of the resultant P-G was also determined (0.72 atom%) based on the survey spectra. The authors attributed the low P doping amount to the large mismatch in atomic sizes between P (100 pm) and C (77 pm) atoms and the unfavorable preparation condition for C–P bond formation.

To confirm the "doping" generation, the high-resolution C 1s, O 1s, or dopants spectra are required and usually some curve fitting (i.e., deconvolution) skills are used to recognize the results. In the same work of above paper, the authors did curve fitting on C 1s peak and four peaks with binding energy of 284.7, 285.2, 286.6, and 290.4 eV were achieved. They were ascribed to sp^2–C, C–P(C–O), C=O, and O–C=O, respectively. To further confirm the phosphorus doping, the high-resolution P 2p spectrum is deconvoluted while three peaks at binding energies of 134.5 eV, 133.5 eV, and 132.0 eV were obtained. These three peaks were ascribed to C–O–PO_3, P–O, and P–C respectively, which confirmed the P incorporation into the graphene matrix. Moreover, the ratios of different doping types were calculated based on the P 2p deconvolution results with the proportions of 13.6%, 34.2%, and 52.2% for each configuration. It's clear that more than half of the doped P species in P-G were P–C type, which explained the superior performance of the P-G catalyst since the P–C binding configuration had been proved to exhibit higher catalytic activity towards I_3^- reduction [56].

The most excellent example for doping type identification by XPS measurement is the nitrogen-doped graphene materials, which have been widely studied and used for many catalytic reactions such as oxygen reduction reaction (ORR). Four main types of nitrogen dopants were identified in nitrogen doped graphene (NG) by deconvoluting the N 1s spectrum (Figure 3). They were assigned to pyridinic N (398.1–399.3 eV), pyrrolic N (399.8–401.2 eV), quaternary (i.e., graphitic) N (401.1–402.7 eV), and pyridinic $^+N–O^-$ (402–405 eV) [57]. As mentioned before, once nitrogen atoms are doped into graphene, C 1s peak would change accordingly. Generally, the peak change shifting to higher energy in the C 1s spectrum indicates the nitrogen successfully incorporates into graphene matrix. For example, in the work of Yan et al. [58], the nitrogen doped graphene quantum dots-$ZnNb_2O_6$/g-C_3N_4 catalysts (NGQDs) were prepared by hydrothermal method and further applied in photocatalytic hydrogen production under visible light. The authors used XPS to examine the chemical composition of the as-synthesized NGQDs. Three predominant peaks at 284.0 eV, 400.0 eV, and 530.6 eV were observed on survey spectra ascribing to C 1s, N 1s, and O 1s, respectively. After curve fitting, the high-resolution C 1s was deconvoluted into five peaks at 284.6 eV, 285.2 eV, 286.6 eV, 287.3 eV, and 289.0 eV, where all peaks shifted to high energy. They corresponded to C–C, C–N, C–O, C=O, and O–C=O, respectively, which meant the nitrogen was present in the catalyst. The deconvolution of high-resolution N 1s confirmed the presence of pyridinc N and pyrrolic N at 398.1 eV and 400.5 eV. Based on these XPS results, the authors concluded that N atoms were successfully incorporated into graphene matrix.

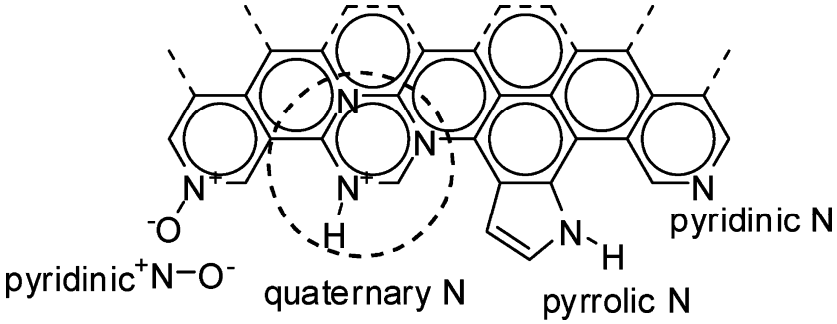

Figure 3. Different nitrogen doping types in nitrogen-doped graphene (Reprinted with permission from ref [34]. Copyright 2012, American Chemical Society).

Another function of XPS on characterizing graphene-based materials in catalysis is to detect active sites and further reveal related reaction mechanism. One good example on this is the illustration of the mechanism of oxygen reduction reaction (ORR) over nitrogen doped graphene (NG) catalysts by direct observation of active sites [59]. Though many simulation results indicated different reaction pathways and adsorption sites for ORR over NG, it's still under controversial on the actual mechanism, which is mainly due to the lack of the direct evidence on the detection of intermediates species or active sites. Xing et al. [59] proposed to determine the active sites on NG by examining its chemical composition change with synchrotron-based XPS before and after ORR. The high-resolution N 1s spectrum exhibited typical pyridinic nitrogen (398.5 eV), pyrrolic nitrogen (399.8 eV), and graphitic nitrogen (401.2 eV) over all three fresh samples (before ORR) with different contents. Based on the XPS results over samples after ORR, the intermediate OH(ads) generating during ORR remained on the carbon atoms neighboring pyridinic nitrogen after ORR. More importantly, there is corresponding relationship between the amount of OH(ads) attachment after ORR and catalytic efficiency. Since OH(ads) should chemically attach to the active sites, the authors concluded that the main active sites for ORR over NG are these carbon atoms adjacent to pyridinic nitrogen while other nitrogen doping configurations are inactive.

XPS has shown its great potential in characterizing graphene-based materials in catalysis especially for heteroatom-doped graphene catalysts. It has become the standard method to prove the successful doping. Almost all reported works related to doped-graphene catalysis adopted it in their characterization part as the first evidence. Simultaneously, two issues are worth paying more attention. First, the information on other heteroatoms (except nitrogen and boron) doping are still limited. It should be very careful to make the ascription of the peak information from XPS for these catalysts. Second, the application of XPS in mechanism exploration for graphene-based catalysis is still at its very early stage and challenges remain including experimental design, effective data collection, and curve fitting skills.

2.3. Fourier Transform Infrared Spectroscopy (FTIR)

Pristine graphene is an allotrope of carbon and no signal can be collected on FTIR [60]. However, as one of the main routes to prepare the practical graphene supports in catalytic research, the oxidation step is essential for the graphite oxide exfoliation. Accordingly, many functional group might be residual in the graphene-based catalysts even after so-called "completely removed", which

leads to severe influence on the catalytic performance [61]. Therefore, it's important to evaluate the reduction level. FTIR is one of the most efficient and facile methods to investigate the residual functional groups [62]. Rout et al. [45] employed rGO as the support for Au−Cu alloy nanoparticles (NPs) as high efficient catalyst for multiple reactions. GO was used as the precursors to load Au−Cu NPs with a one-pot deposition-precipitation method while the reduction of GO to rGO occurred simultaneously. With FTIR, the typical peaks corresponding to functional groups in GO included O–H stretching (3400 cm^{-1}), C–H stretching (2910 cm^{-1}), C=O stretching (1687, 1710 cm^{-1}), C=C stretching (1542, 1568 cm^{-1}), C–O stretching (1208 cm^{-1}), C–OH stretching (1113 cm^{-1}), C–O–H bending (1409 cm^{-1}), and C–H system stretching (2875 cm^{-1}). All of these characteristic signals become much weaker while some of them were even disappeared over Au–Cu/rGO, which indicated the significant reduction of GO to rGO. Moreover, the authors used Raman to further confirm the efficient removal of functional groups from GO and indicate the formation of rGO.

Due to the difference of preparation condition and interaction between catalytic active species and graphene supports, the positions of the characteristic peaks from the functional groups may shift slightly. Hu et al. [21] prepared the MnO_2/graphene composites through the direct redox reaction between graphene oxide and potassium permanganate under hydrothermal condition, which aimed to catalytic degradation of toluene with ozone. They analyzed the as-synthesized MnO_2/graphene catalysts by FTIR as shown in Figure 4. Absorption peaks C=O at 1719 cm^{-1}, aromatic C=C at 1619 cm^{-1}, epoxy C–O at 1222 cm^{-1}, and alkoxy C–O at 1042 cm^{-1} were observed in the case of GO. After hydrothermal treatment, the peaks at 1719, 1619, 1222, and 1042 cm^{-1} diminished or decreased dramatically over reduced graphene oxide and MnO_2/graphene composites. Thus, the authors concluded that the oxy-functional groups were removed under hydrothermal condition. Moreover, a new peak at around 707 cm^{-1} was observed in some of the MnO_2/graphene catalysts. The authors ascribed it to the vibration mode of the Mn–O–C bond, resulting from interactional reaction between carbon of GO and MnO_4^- ions. They proposed that the presence of Mn–O–C bond confirmed the intimate contact existing between graphene and MnO_2, which would facilitate adjacent attack among the reaction intermediates [21].

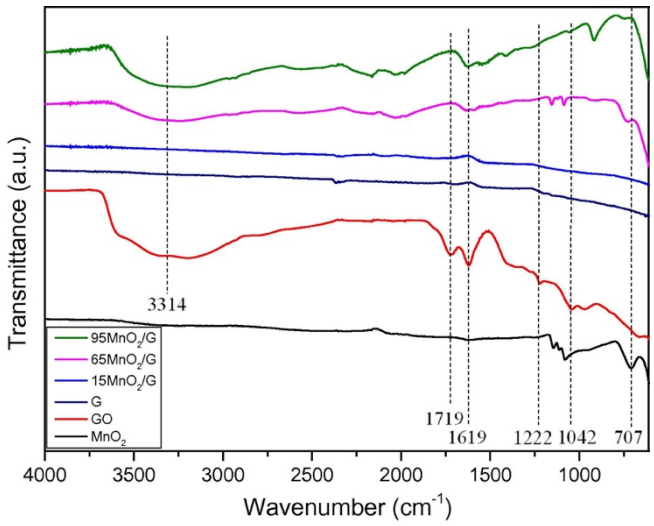

Figure 4. FTIR spectra of GO and reduced GO supported catalysts (Reprinted with permission from ref [21]. Copyright 2014, Elsevier).

The application of FTIR for investigating the structural integrity of graphene-based catalysts was widely adopted. It's worth noting that the FTIR result is only partial evidence for the residual determination due to the detection limitation of the instrument. It's highly recommended to combine with other techniques such as Raman, XPS, and X-ray diffraction (XRD) to further confirm the information.

2.4. X-ray Techniques: XRD, XANES, XAFS, and EXAFS

X-ray diffraction (XRD) and X-ray absorption near edge spectroscopy (XANES) measurements are informative tools to probe the structure, oxidation state, and local symmetry, which is beneficial for investigating crystalline structure, an important parameter for catalyst [63,64]. In addition, extended X-ray absorption fine structure (EXAFS), with respect to bond lengths and coordination numbers, is also considered as a powerful method [65]. Moreover, these X-ray techniques are employed to estimate the size and distribution of loading sites and in turn to assess the catalytic sites dispersion, which governs the catalytic performance of a given material to a great extent.

Generally, the peak at 2θ of ~26° for pristine graphite and that at 2θ of ~11° from the graphene oxide are the common XRD results over graphene-based catalysts. In the work of Nguyen et al. [66], frost-like CuO combined graphene–TiO_2 was proposed as the catalyst for photocatalytic degradation of organic pollutants in water. XRD was employed to analyze the crystalline phase and further assess the purity and crystalline size of the CuO, CuO–TiO_2 nanocomposite. The typical diffraction signals for graphene, CuO, and TiO_2 were detected. The presence of graphene was demonstrated by the observation of the peak at 2θ of 25.9°, referring to (002) reflection, over CuO–graphene and CuO–graphene–TiO_2 composites. The loading of catalytic species was confirmed by the clear distribution of the peaks attributed to polycrystalline monoclinic CuO phase corresponding to (110), (111), (111), (202), (020), (202), (311), (220), (311), (222), and (222). Finally, the existence of anatase TiO_2 was supported by the peaks ascribed to (101) and (200).

One of the important function of X-ray diffraction (XRD) in characterizing graphene-based catalysts is to confirm the reduction of GO to graphene. Li et al. [67] fabricated reduced graphene oxide/g-C_3N_4 composites membranes to catalytically degrade organic contaminants and separate oil-in-water emulsion. X-ray diffraction (XRD) was performed on GO, rGO/poly-dopamine (PDA), g-C_3N_4, and rGO/PDA/g-C_3N_4 composites. A strong diffraction peak at 11.5° was observed over GO, corresponding to the (001) plane. Remarkably, it disappeared on the rGO/PDA while two broad peaks at around 26.5° and 43.6° were observed. The disappearance of the former peak indicated the reduction of exfoliated GO sheet by dopamine to rGO. The reduction would lead to the significant decrease of oxy-containing functional groups and increase of layer-layer stacking, which supported by later two peaks. In the case of rGO/PDA/g-C_3N_4, the characteristic diffraction peak of GO shifted to 10.5° while the intensity became much weaker and the peak width increased dramatically, which also demonstrated the partial reduction of GO in this catalyst. Hu et al. [21] also used XRD to confirm the reduction of GO to graphene. Compared with the exfoliated GO, the authors found that diffraction peaks of graphene disappeared at 10.1° (001) while small bump near 24.5° (002) was observed. They concluded that GO was successfully converted to graphene based on this information. With XRD pattern, the layer number of graphene can also be determined by combining Scherrer equation with Lorentzian fitting over the (002) reflection [68], which may be used to supplement the

results from other techniques on layer number determination such as atomic force microscopy (AFM).

With X-ray absorption fine structure (XAFS) and extended X-ray absorption fine structure (EXAFS) spectroscopy, the accurate percentage of specific bonds, which is important for interpreting the catalytic reaction performance, could be characterized over graphene-based catalysts. Leng et al. [69] designed Co_3O_4/graphene nanocomposites for oxygen evolution reaction (OER) based on the prediction of theoretical calculations. The desired catalyst should contain optimized percentage of Co–O–C bonds, which was estimated experimentally by XAFS and EXAFS measurements in their work. Co K-edge XANES showed that compared to that of the pure Co_3O_4 the absorption edge of Co_3O_4/graphene composite A shifted to lower energy, indicating the charge transfer from C to Co within the composite. With pre-exclusion of Co–C bonding from XPS results, the authors proposed the presence of Co–O–C bond. This assumption was also supported from their Fourier transform (FT) data, where clear shift of the Co–O bond from Co_3O_4/graphene A was observed. The shift suggested the lattice distortion of Co_3O_4, which resulted from the rGO-Co_3O_4 interaction. Then, the detailed structural information of the Co–O bond was collected by EXAFS. Two kinds of Co–O bonds were revealed in Co_3O_4/graphene composite A with one at ~1.87 Å while the other at ~2.04 Å. By comparing to the Co–O bond length (1.89 Å) of Co_3O_4, the authors concluded that the short one belonged to Co–O–Co, while the longer one came from Co–O–C. With these results, they confirmed the existence of Co–O–C bond in composite A. Furthermore, they estimated the ratio of Co–O–C to Co–O was 43:57 based on the intensity of two peaks. They used the same method to calculate the ratio over other two composites B and C with different Co_3O_4 loadings. And higher percentage (61:39) of Co–O–C bond was observed on the lower loading one (C) while that of higher loading catalyst (B) exhibited lower percentage of Co–O–C bond due to the merging of most of the Co_3O_4 nanoparticles in catalyst B. The OER reaction test showed that catalyst A with optimized ratio of Co–O–C bond possessed the highest activity, which was consistent with the simulation results.

Annamalai et al. [70] employed XANES and EXAFS functions for Fe K-edges to analyze bulk local structure of as-prepared FTO/α-Fe_2O_3 and FTO/GO/α-Fe_2O_3 catalysts. Compared to reference α-Fe_2O_3, the same XANES spectra were observed on the catalysts. The quadrupole transition of 1s → 3d with pre-edge peak at 7115 eV was observed while the absorption rising feature and energy positions were also the same. The similar results were also collected over EXAFS spectra. The minor difference was observed on the increase of the intensities in the peaks at 0.8–2.0 and 2.1–3.9 Å. The authors proposed attributed it to the enhanced ordering of the nearest Fe–O bond and complicated Fe–Fe and Fe–O bonds, respectively, which is generally observed for the films on substrate. Based on these XANES and EXAFS results, they concluded that graphene oxide layer showed insignificant effect on the structure of α-Fe_2O_3 in an angstrom order.

Metal-free catalyst is one of the hottest topics of graphene-based catalysis in recent years. As mentioned in XPS section, understanding of active sites at the atomic-level is very important for designing highly active and stable metal-free catalysts. Though XPS has shown excellent ability on illustrating the mechanism of oxygen reduction reaction (ORR) over nitrogen doped graphene (NG) [59], its application over sulfur doped one is limited due to the difficulty of exploring sulfur content by XPS [71]. Alternately, sulfur K-edge X-ray absorption near edge spectroscopy (XANES) is able to provide precise information about the nature of doped sulfur. Therefore, sulfur K-edge XANES can be a helpful tool for identification of the active sites and exploration of the mechanism.

For example, El-Sawy et al. [71] used XANES to illustrate the active sites of a sulfur doped carbon nanotube-graphene nanolobes catalyst in oxygen evolution reaction (OER) and oxygen reduction reaction (ORR). The authors synthesized the catalyst by a sequential bidoping strategy, which introduced stable sulfur–carbon active-sites. Two broad peaks corresponding to reduced (S_{Red}) and oxidized (S_{Ox}) sulfur species were observed on the sulfur K-edge XANES spectra (Figure 5). The authors considered that S_{Red} consisting of three different functionalities: exocyclic sulfur (sulfur out of the carbon six-member ring), heterocyclic sulfur (sulfur in the ring), and sulfoxide (–SO–), while the S_{Ox} peak was contributed from sulfone ($–SO_2–$) and sulfonate ($–SO_3$). Compared to other two "single-doped" sulfur samples (S-CNT 180 °C and S"-CNT 1000 °C), the "bi-doped" catalyst (S,S"-CNT 1000 °C) had the highest normalized intensity for both S_{Red} and S_{Ox} peaks. The OER and ORR test confirmed that increasing the incorporation of heterocyclic sulfur into the carbon ring not only promoted OER and ORR activity, but also enhanced the stability. Combining with other techniques including scanning transmission electron microscopy electron energy loss spectroscopy (STEM-EELS), XPS, Raman, and high-angle annular dark-field scanning transmission electron microscopy (HAADFSTEM), the authors built the correlation of the superior activity and stability of the synthesized catalyst with the increasing of sulfur doping, which successfully revealed the promotion mechanism of sulfur doped carbon nanotube–graphene nanolobes.

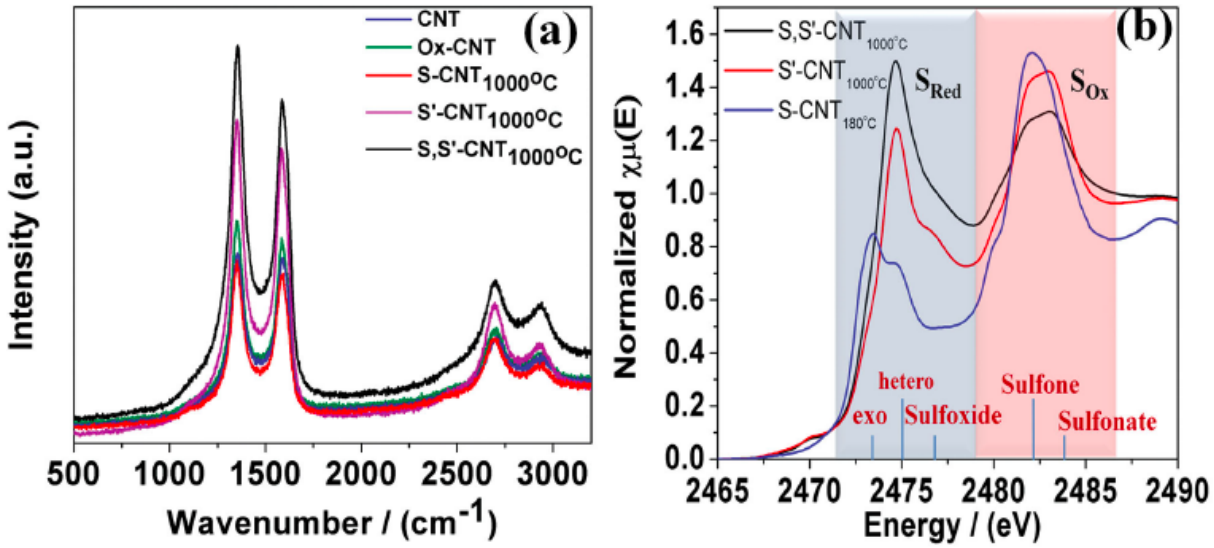

Figure 5. (a) Raman spectra and (b) Sulfur K-edge X-ray absorption near edge spectroscopy (XANES) for sulfur doped carbon nanotube–graphene nanolobes (Reprinted with permission from ref [71]. Copyright 2016, John Wiley & Sons, Inc).

The application of XRD for phase determination and confirming the reduction of GO to graphene is the most convenient tool among the above X-ray techniques. Obviously, it's inferior to the later three approaches due to the limited information collected on it. Therefore, its application is always accompanied with other methods such as Raman, XPS, and FTIR etc. XANES, XAFS, and EXAFS can provide lots of information to characterizing both catalyst structure and reaction mechanism, while the access to them is a common issue for most researchers.

2.5. Atomic Force Microscopy (AFM)

Due to its convenience and reliability, AFM is regarded as the leading approach for thickness measurement and the layer number counting. In a typical measurement, it utilizes a cantilever with a sharp tip (~5–10 nm) that scans across the surface of graphene-based materials. The sensitive changes in vibration amplitude and frequency of the tip are collected due to the subtle changes in heterogeneity of the surface, which can analyze the topography of the sample. The obtained three-dimensional images enable the measurement of the thickness of graphene films. In consideration of that the perfect graphene has a single atom thickness of around 0.35 nm, thus, the number of the layers could be counted. For example, Yang et al. [72] designed a monolayer graphene-based Fe/N/C model catalyst (FeN-MLG) to explore the active sites of pyrolyzed Fe/N/C, the most promising non-precious-metal catalysts for oxygen reduction reaction (ORR). The highly heterogeneous structures formed during the pyrolysis process in conventional catalysts usually make the probe of the active sites difficult. The authors proposed to use single layer system reveal the mechanism. AFM was adopted by them as the leading tools to clarify the successful synthesis of desired catalyst (Figure 6). Figure 6A displayed the AFM image of a folded FeN-MLG. Figure 6C demonstrated the corresponding height profile, indicating that the thickness of the layer of FeN-MLG is ~0.5 nm. Therefore, they concluded that the synthesized catalyst consisted of a single atomic layer although the thickness is slightly higher than the expected value (0.35 nm).

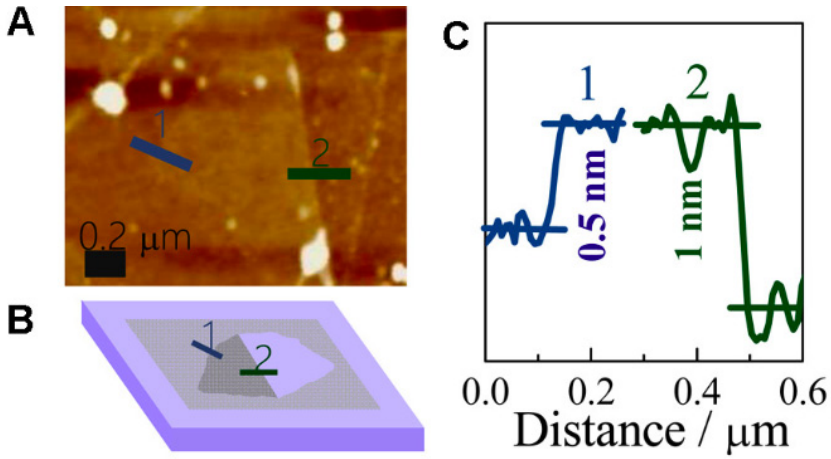

Figure 6. AFM measurement of folded FeN-MLG. (A) AFM image. (B) Bright spot morphology schematic. (C) Height profile marked by the solid lines 1 and 2, respectively, showing that the thickness of FeN-MLG is about 0.5 nm (Reprinted with permission from ref [72]. Copyright 2017, American Chemical Society).

Another function of AFM for characterizing graphene-based catalysts is to determine the surface roughness, which could provide some information of surface area and the active area. Song et al. [73] prepared Pd–Fe/graphene catalysts by photocatalytic reduction and further tested its performance for electrochemical oxidation-reduction properties for chlorophenols. The AFM image of the $Pd_{0.5}Fe_{0.5}$/graphene catalyst revealed that the catalyst was an irregular crystal block with an average thickness of approximately 1.2 nm. More importantly, the authors determined the average roughness of the sample sheets was 0.175 nm. Based on the information of rough surface, they

concluded that the bimetallic Pd–Fe nanoparticles formed on the graphene surface and further provided a larger number of active sites.

The major issue with imaging one atom thick materials (graphene) is that there is rarely a perfect contact between the tip and sample. In addition, image feedback settings and surface chemistry also affect the results [74]. Accordingly, although AFM was widely used for thickness determination and number of layer counting, a wide range of measured values (0.4–1.7 nm) were reported in the literature for the thickness of single layer graphene, indicating its inaccuracy. Thus, it's necessary to mention that the high experimental skill is required when using AFM to measure the thickness and further count the number of layer of graphene-based catalysts since the abovementioned result is often the case.

2.6. SEM, TEM, and HRTEM

Scanning electron microscopy (SEM), transmission electron microscopy (TEM), and high-resolution transmission electron microscopy (HRTEM) are usually employed to visualize the morphology and structure of graphene-based catalysts, which provides lots of information to rationalize their catalytic performance [75]. For example, Lu et al. [76] used graphene–MnO_2 hybrid nanostructure as catalyst for formaldehyde oxidation (Figure 7). SEM of graphene demonstrated 2D planar structure with a well-defined and interconnected porous network. The authors proposed that this 2D planar architecture facilitated the adsorption of reagents and exposed more active sites for catalysis. In addition, the obvious wrinkles and folds revealed the flexibility of graphene nanosheets. Small MnO_2 nanoparticles were observed uniformly dispersed on the graphene surface, while they exhibited nanoneedle shape as indicated by TEM and HRTEM images. The authors attributed high dispersion of MnO_2 to the planar architecture of graphene nanosheets, while the loaded MnO_2 nanoneedles acting as nanoscale spacers in turn prevented the graphene nanosheets from aggregation to some extent. The d-spacing of 0.70 nm was determined from HRTEM image and assigned to MnO_2 (003), which confirmed the crystalline feature of MnO_2 nanoneedles.

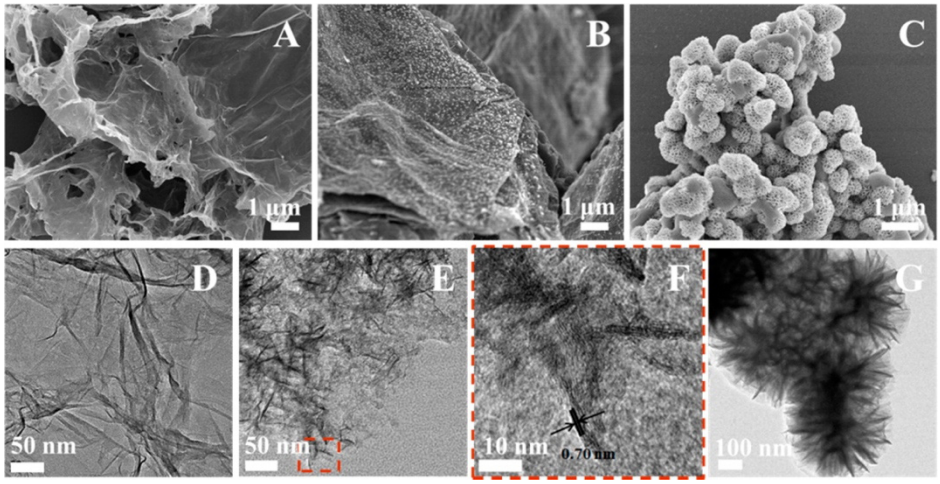

Figure 7. SEM and TEM images of graphene (A, D), graphene-MnO_2 (B, E), and MnO_2 samples (C, G); (F) HRTEM image of graphene–MnO_2 (Reprinted with permission from ref [76]. Copyright 2016, American Chemical Society).

Energy dispersive spectrometry (EDS) provided with FE-SEM is usually used for elemental composition survey. Theerthagiri et al. [77] synthesized diselenide nanorods on graphene oxide nanosheets as advanced electrocatalyst for hydrogen evolution reaction (HER). The authors used EDS to determine the elemental composition of pure $FeSe_2$, GO and optimized 30% $FeSe_2$/GO composites. The EDS spectrum evidently confirmed that the $FeSe_2$ sample comprised of Fe and Se atoms, whereas GO was composed of C and O atoms only. Also, the EDS spectrum of $FeSe_2$/GO revealed the existence of Fe, Se, C and O atoms only. Moreover, the atomic percentages of species were achieved. Based on these results, they concluded that the both $FeSe_2$ and GO were present in composite sample. Kashinath et al. [78] proposed a sol-gel assisted hydrothermal method to synthesize the hybrid ZnS–rGO nanocomposite for efficient photodegradation of dyes. The authors also used EDS to investigate the elemental composition. EDS analysis confirmed that the elemental ratio of the as-synthesized hybrid nanoparticles was stoichiometric for the component zinc and sulfur atoms respectively while the percentage of reduced graphene oxide (carbon to oxygen) ratio was in proportion. Moreover, they found that the ratio and percentage of carbon to oxygen decreased with increase in doping molar ratio of ZnS precursors.

HRTEM is also an effective method to detect surface defects of graphene-based catalysts. For example, Wei et al. [79] synthesized a novel cobalt encapsulated in N-doped graphene layers (CoO_x@CN) catalyst for catalytic hydrogenation of quinoline compounds, which exhibited high efficiency and stability. HRTEM demonstrated that Co NPs were well encapsulated inside the graphene layers. Moreover, obvious defects like small channels were also observed on the surrounded graphene layers, which were believed to facilitate the reaction. The authors also measured the pore-size distribution and typical mesoporous structure (pore size ~12 nm) was observed. In addition, BET surface area was determined to be 531 $m^2 \cdot g^{-1}$. The large surface area and the mesoporous pores partially supported the HRTEM observations.

Moreover, HRTEM elemental mapping is a powerful tool to detect the element distribution of graphene-based catalysts. For example, Vij et al. [80] reported one noble metal-free, nitrogen and sulfur codoped graphene/carbon nanotube decorated with Co nanoparticles (NPs) catalyst for oxygen reduction reaction (ORR). The uniform distribution of Co NPs and doped nitrogen and sulfur was clearly observed by HRTEM elemental mapping at different magnification. Although the detection of sulfur atoms at low magnification was not feasible due to the very low doping percentage of sulfur, they exhibited clear images at very high magnification.

Another important function of these visual tools on graphene-based catalyst characterization is determining the number of graphene layers, which directly determines the surface area of the catalyst and further affects their catalytic performance dramatically [61]. In practical application of graphene-based materials in catalysis, layer folding is often the case. With TEM image of the folds formed at the edge, one can generate flake thickness statistics. Therefore, the estimated thickness of a graphene sample can be determined. Accordingly, the number of layers can be calculated [81]. The other direct method is the observation of the edges by HRTEM, which provides an accurate way to count the number of layers at multiple locations on the layer-structure catalyst [82,83]. Another way to measure the number of layer is with selective area electron diffraction (SAED), the crystallographic technique equipped inside a TEM. Graphene-based materials with different number of layer would display various dark line, which could be used to determine the layer number [81].

2.7. UV-vis, XRF, ICP, and TGA

As the most widely investigated method for graphene-based catalysts preparation, the approach using exfoliated graphite oxide as precursor followed by post-treatment with catalytically active species can obtain high yields of graphene-based materials. The first step is to harvest exfoliated graphite oxide (i.e., graphene oxide) dispersion in aqueous, while ultraviolet-visible spectroscopy (UV-vis) is the most convenient way to confirm the successful synthesis. The graphitic structure shows an absorption peak at ~262 nm while a monolayer of GO exhibits absorption at ~230 nm in UV-vis spectrum, which is attributed to the π–π* transitions of aromatic C–C bonds. Based on this difference, one can easily determine the quality of their "GO" products. Zhou et al. [84] used UV-vis spectra to study synthesized GO and observed the absorption peak at 227 nm and a red shift to 254 nm after hydrothermal reduction treatment (Figure 8). Moreover, the authors considered that the increase of absorption in the whole spectral region (>238 nm) indicated the restoration of π-conjugation network within graphene nanosheets. It's worth noting that the concentration of the GO dispersion against the UV-vis measurement should be low to less than 0.1 mg/ml. Otherwise, the fluorescent interference would affect the results dramatically.

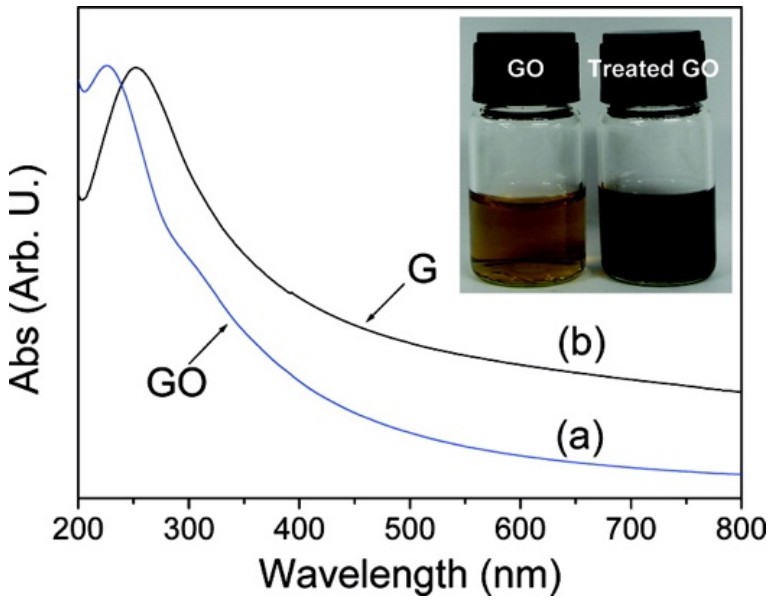

Figure 8. UV-vis spectra of the GO (a) before and (b) after hydrothermal treatment. Inset shows the color change GO dispersion (Reprinted with permission from ref [84]. Copyright 2009, American Chemical Society).

The ''metal-free'' concept mentioned above was built on the fact that no metal was intentionally added during the catalyst preparation procedure. However, both main preparation methods (graphite oxide exfoliation and chemical vapor deposition (CVD)) for graphene-based "metal-free" catalyst synthesis involve possible metal residual. $KMnO_4$ is always introduced in the former method [85,86], while the catalytic metal substrate is required in the CVD process [87,88]. Even with the long-time-consuming washing or chemical etching, the complete removal of the metal substrate cannot be guaranteed [89]. Simultaneously, reported studies already proved that the metal impurities

even in a trace level had beneficial impact on catalytic activity [90,91,92]. Therefore, the possible presence of residual metals in the produced graphene-based catalysts should be excluded before making such "metal-free" claim. X-ray fluorescence (XRF, non-destructive) and inductively coupled plasma mass spectrometry (ICP, destructive) are two highly recommended tools to analyze the residual metal concentration in the graphene-based catalysts prior to further investigation.

One major concern with graphite oxide exfoliation method for graphene-based catalyst preparation is the insufficient oxidation of graphite [5,93]. It would lead to incomplete exfoliation of graphite and decrease the level of individual graphene sheets while aggregated "graphene" would be achieved. Usually these unsuccessful products show inferior the reaction performance. Therefore, it's necessary to check the degree of oxidation of the "exfoliated graphite oxide" before using for the catalyst synthesis. One facile and practical technique is thermogravimetric analysis (TGA). It can analyze the mass loss of the function groups quantitatively, which were produced in the oxidation procedure. With this information, one can determine the degree. In addition, combining TGA with FTIR or mass spectra (MS), much more accurate informative data may be achieved.

The above four techniques are related to the graphene-based catalyst preparation. Although the detection mechanisms are simple, their applications would help to clarify many concerns about graphene-based catalysis.

2.8. Other Techniques

Catalyst surface area is one critical parameter in catalysis. Except affecting by the conventional pore structure, it's also related to the layer number in graphene-based catalysts [94]. Therefore, the determination of layer number can be partially used to represent the surface area condition and vice versa. Brunauer–Emmett–Teller (BET) surface obtained from nitrogen adsorption-desorption at 77 K could measure the surface area efficiently and reliably, which can offer some indirect support for the layer number identification qualitatively. The theoretical calculations indicate that the highest surface area of a monolayer graphene is 2630 m^2/g. Due to the random agglomeration, stack, and overlap of exfoliated graphene sheets, in practical application, the actual areas of graphene-based catalysts are usually much lower than the value. It would be good practice to compare the layer number of different samples by looking at the surface area data [21].

As mentioned before, defects influence the reaction performance greatly, which results into the importance of their analysis and detection. Scanning Tunneling Microscopy (STM) images are powerful in determining morphology, which may be used to represent the defect condition. This technique is to probe the charge density (at the Fermi level) of the lowest unoccupied or highest occupied states of the sample. The signal can be collected by applying different bias voltage (V_{bias}) between the tip and specimen, which leads to the change of electrons moving direction. Similar to AFM, for atomic resolution images of graphene-based materials sharp tip is required. The applications of this technique keep increasing. For example, the electronic properties of nitrogen doped graphene were investigated by both theoretical simulation [95] and experimental study [42].

Above are the main techniques for characterizing the bulk and surface structure of graphene-based catalyst. They have been adopted in different catalytic systems and showed great promotion for catalytic research. Several points are worth noting. First, it highly recommended to combine more than three tools in one's study to investigate the properties since one or two techniques may show partial information and sometimes mislead the direction. Second, deep data

mining over collected results is helpful to take full advantage of the potential of some tools such as the case of 2D peak deconvolution in Raman and active sites determination in XPS. Third, several tools such as ICP and XRF for characterizing absence of metal are underestimated, which are actually very helpful for clarifying specific concerns. Fourth, due to the novel and unprecedented structure, the data accumulation over graphene-based catalysts is limited. Lots of new results collecting over various instrument keep increasing. Simultaneously, it should be very careful to make any conclusion before comprehensive investigations such as combination with other tools or theoretical computations.

3. Chemisorption Ability Determination

The techniques for determining chemisorption ability of graphene-based catalysts are similar to the conventional catalysis. However, their usage in graphene-based catalysis is much less than those of later. It may be due to that most attentions of graphene-based catalysis focused on materials innovation, leading to the structure characterization plays the most important role. Here we introduced several tools reported in literature while suggestions were also offered.

3.1. Diffuse Reflectance Fourier Transform Infrared Spectroscopy (DRIFTS)

One very important theory in catalysis is the heterogeneous acid-base catalysis, which was transferred from homogeneous system. Surface acidity/basicity can influence catalytic performance dramatically by changing adsorption strength and type [96,97,98]. In some cases, acidity/basicity of the surface active phase is even considered as a key factor that influences catalytic performance [99,100,101]. The two of the most important concepts in heterogeneous acid-base catalysis are Lewis and Brønsted acid-base theory, which were applied to solid surfaces to determine surface acidity or basicity. The definitions of these two are completely different. The former one focuses on electron donation/acceptance while the Bronsted involves proton (H^+ ion) transfer, which indicates the different adsorption mechanism. It's necessary to distinguish the Brønsted and Lewis acid sites on catalyst surface, which is crucial to explore mechanism of a catalytic reaction. Diffuse Reflectance Fourier Transform Infrared Spectroscopy (DRIFTS) is a powerful tool to achieve this goal by differentiating vibrational bands of the adsorbed basic probe molecules. Wang et al. [102] found that GO could be a facile acid catalyst for the conversion of carbohydrates into 5-ethoxymethylfurfural (EMF). Furthermore, the types of acid sites in GO was observed to play crucial role in the reaction. The authors used DRIFTS to investigate the underlying mechanism with NH_3 as a probe molecule. They first identified the two types of acid sites in GO based on the characteristic bands. Peaks at ~1410 and ~1730 cm^{-1}, were ascribed to Brønsted acid sites, which are from the formed NH_4^+ due to the interaction between Brønsted acid sites and NH_3 molecules. Peak at ~1600 cm^{-1} was attributed to Lewis acid sites due to the coordination of NH_3 to the Lewis acid sites. The signal intensity of catalyst before and after reaction was then compared. It's observed that those from Brønsted acid sites reduced while those of Lewis acid sites increased. The authors ascribed this change to the partial removal of carboxyl groups (Brønsted acid sites) and other oxy-functional groups due to heat treatment during the catalytic reaction. The removal also increased some electron vacancies, which created additional Lewis acid sites.

DRIFTS can also be used for detecting active-sites condition. Xiao et al. [103] proposed few layer graphene supported ruthenium catalysts (Ru/FLG) for the conversion of levulinic acid (LA) to γ-valerolactone (GVL), which showed both high conversion (99.7%) and selectivity (100%) and demonstrated 4 times higher activity and exceptional stability comparing to commercial activated carbon supported ruthenium catalysts (Ru/C). In consideration of the same metal and loading on the catalysts, the authors attributed the superior performance to the different condition of Ru active-sites and they proved it with DRIFTS using CO as the probe molecule. Only one single CO adsorption peak at 1977 cm^{-1} was observed on Ru/FLG while two peaks were found at 1977 and 2038 cm^{-1}, respectively, over Ru/C (Figure 9). The disappearance of the CO adsorption peak at 2038 cm^{-1} on the Ru/FLG indicated it only possessed electron-rich Ru(0) atoms, which would donate more d-band electrons to the π* orbital of adsorbed CO molecules. Based on this chemisorption results, the authors conclude that these electron-rich Ru(0) atoms facilitated the activation of the hydrogen molecule and finally promoted the hydrogenation activity.

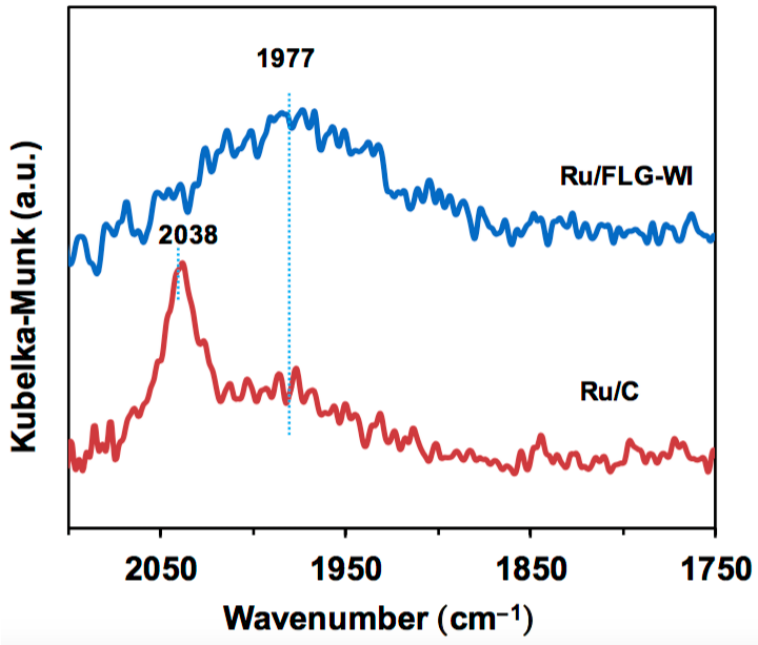

Figure 9. DRIFTs spectra of CO adsorption on graphene supported Ru (Ru/FLG-WI) and activated carbon supported Ru (Ru/C) catalysts (Reprinted with permission from ref [103]. Copyright 2016, American Chemical Society).

3.2. Other Techniques

Several other techniques reported in literature on chemisorption ability determination include temperature programmed reduction (TPR), CO chemisorption, and NH_3/CO_2-temperature programmed desorption (TPD). For a metal supported on graphene catalyst, temperature programmed reduction (TPR) is usually employed to study the oxidation state of the metal species as well as the related metal-graphene (and its derivatives) interactions, which may can be used for chemisorption ability determination [104,105]. CO chemisorption is the most convenient and reliable method for surface active-site detection. It's also adopted in graphene-based catalysis, where the

natures of active sites (dispersion and amount) were further elucidated [106,107,108]. Different from DRIFTS, NH_3/CO_2-TPD is a reliable and convenient tool to measure the total acidity/basicity of a catalyst, which is also an important parameter of catalyst surface. Its application in graphene-base catalysis was also reported in several papers [109,110,111].

In summary, the research on chemisorption ability determination in graphene-based catalysis is rarely reported. Most of reported work in literature used conventional tools to obtain related information. Since the chemisorption ability plays the crucial role in determining catalytic performance, it's necessary to adopt more or develop new techniques to characterize this important property. Otherwise, the exploration of the intrinsic mechanism in graphene-based catalysis would be difficult. Many works reported that π–π interaction between graphene-base catalysts and reactants with aromatic chromophore facilitated the chemisorption and finally promoted the reaction performance [62,112–115]. However, there is no direct evidence to support this speculation.

4. Reaction Mechanism Investigation

Basically, there are three main types of approach to explore the reaction mechanism in graphene-based catalysis: 1) studying mechanism by experimental techniques based on the above bulk and surface structure analysis and chemisorption ability determination; 2) theoretical computations with density functional theory (DFT); 3) combination of both experimental and theoretical.

4.1. Experimental Observations

Exploration of catalytic mechanism with experimental observations is the most used approach for all catalytic research including graphene-based catalysis. Since the bulk and surface structure analysis and chemisorption ability determination have provided lots of information to help us reveal the reaction mechanism. For example, Nie et al. [116] used N-doped reduced graphene oxides (N-rGO) supported ultrafine Pd nanoparticles (NPs) (Pd/N-rGO) as catalyst for selective hydrogenation of C=C bond of unsaturated hydrocarbons. Under mild condition, Pd/N-rGO showed high activity and selectivity for the hydrogenation of C=C bond in cinnamaldehyde and hydrogenation of phenol to cyclohexanone. The authors used several techniques to investigate the mechanism. XRD, XPS, and TEM confirmed that the interaction between N-rGO and Pd enhanced with the amount of nitrogen atoms in N-rGO. More importantly, this enhanced interaction resulted into the high dispersion of Pd. Therefore, they attributed the superior activity to the nitrogen doping. The reason for the high selectivity was also revealed with experimental measurements. The author conducted Raman analysis over sample after adsorption of cinnamaldehyde. The obtained spectra suggested that N species doped in the matrix of graphene could anchor single bond –CHO group while activate the C=C bond in the same molecular, which finally improved the selectivity.

In the work of Xiao et al. [103], few-layer graphene (FLG) supported ruthenium nanoparticle catalyst (Ru/FLG) showed both high conversion (99.7%) and selectivity (100%) for conversion of levulinic acid (LA) to γ-valerolactone γ-valerolactone (GVL) at room temperature. It demonstrated 4 times higher activity and exceptional stability comparing to traditional activated carbon supported ruthenium catalysts (Ru/C). To understand the mechanism, the authors first characterized the structure of the catalysts by several tools. The TEM images of Ru/FLG illustrated uniformly

dispersed Ru nanoparticles on the graphene sheet without any aggregation. (002) peak at 11.3° and broad peak at 26.2° were observed on XRD patterns of graphite oxide and FLG respectively. The former peak indicated an interlayer separation of about 7.8 Å while the later peak suggested the reduction of GO and some amounts of stacking. The BET surface area of FLG was determined to be 420 m^2/g. This value is far below than the theoretical value for a graphene monolayer (2630 m^2/g). Therefore, the authors concluded that the multilayer graphene support was used in this work. The overlap of Ru 3d and C 1s bands make it difficult to use XPS on characterizing the oxidation state of Ru. The XANES was adopted to determine the state distribution (46.2% Ru(0) and 53.8% Ru(IV) on Ru/FLG catalyst). The authors further proposed that the enhanced activity and stability can be attributed to the interaction between graphene and Ru nanoparticles, which facilitated greater metallic Ru content generation. And they used several techniques, including XPS, FTIR, and Raman spectroscopy to support this assumption. XPS Ru 3p spectra showed that Ru/FLG had a lower binding energy (462.6 eV) and higher concentration of Ru(0) (36.8%) compared to Ru/AC (462.8 eV and 29.4%, respectively). DRIFTS with CO as probe was also performed and confirmed Ru/FLG had higher concentration of Ru(0). DRIFTS results further proved that Ru/FLG only possessed electron-rich Ru(0) atoms at defect sites, which was supported by the ratio of the intensities of D and G bands from Raman spectroscopy. Finally, the author concluded that the interaction between graphene and Ru upshifted the d band center of Ru, which facilitated the activation of the hydrogen molecule and finally promoted the hydrogenation activity. The strong interaction between Ru and graphene defect sites also prevented the leaching and migration of Ru NPs, which explained the superior stability of Ru/FLG compared to Ru/C.

Experimental observations can provide direct evidence to support the proposed mechanism, which lead to the more solid conclusion than the theoretical results. One reasonable mechanism usually is built on a series of characterization results with comprehensive analysis. Thus, this approach would be a long-time-consuming process due to the careful data collection and the more important and complex data interpretation.

4.2. Density Functional Theory Computations (DFT)

DFT has been widely adopted for describing and predicting the chemical and physical properties of pure and hybridized materials [117,118,119]. With DFT computations, many graphene-based materials have been explored and designed. More importantly, lots of fantastic properties are disclosed, especially when some of them are unable to be revealed by experimental tools. Two main classes of standard DFT, plane-wave DFT (like Quantum ESPRESSO [120], ABINIT [121], VASP [122], SIESTA [122], and CASTEP [123]) and local orbitals DFT (such as TURBOMOLE [124], Gaussian [125], and ADF [126]), have been employed for graphene-based catalysis. The results from DFT computations over graphene-based catalysts have been widely utilized to investigate adsorption and activation mechanism [127], calculate activation energy [128], determine the rate-limiting step [129] and active sites [130], and discuss catalytic pathway [131], which covers almost all catalysis related topics. For example, DFT was used to study the mechanism of the selective oxidation of alcohols to aldehydes and ketones over the model metal-free nitrogen-doped graphene (NG) catalyst [132]. The authors used M06-2X/6-31+g** level of theory (Gaussian 09 software package) to optimize all of the geometries without any constraints. First, four models of graphene were initially taken to benchmark the catalytic properties of graphene with both

hydrogenation energies and band gap of graphene as the screening parameter to select suitable graphene model. Then Model-4 was taken and doped with nitrogen atom at the edge and at the center, based on the reported information from previous studies. It was found that different activated oxygen species (AOS), depending on the position of N-doping, could be generated due to the activation of dioxygen on NG. Moreover, the oxidation reaction can perform on all three AOS. However, the overall barrier of the reaction over aromatic alcohols was found lower at ketonic oxygen (Sub_K) while that over aliphatic alcohols was at the center (Sub_C) (Figure 10) [132].

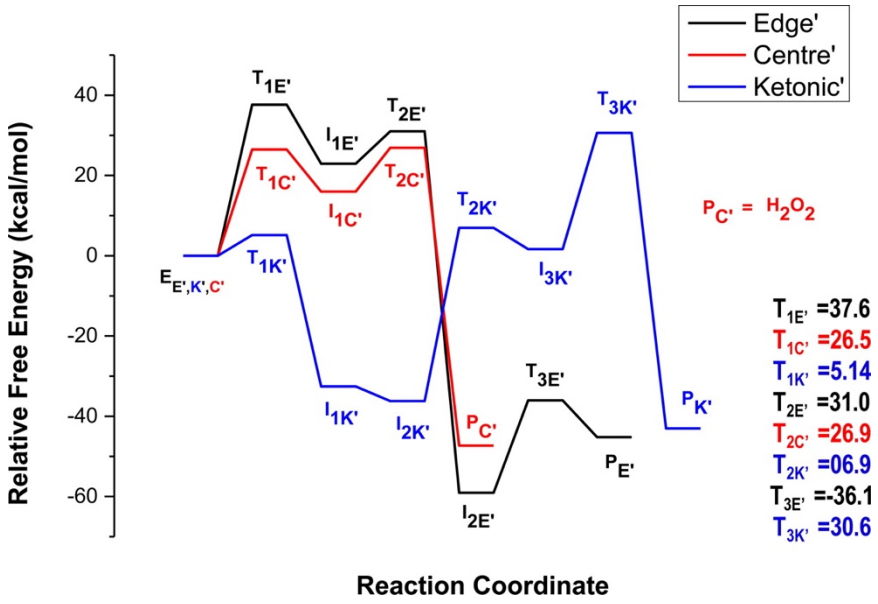

Figure 10. Reaction profile for the proposed oxidation reaction of benzyl alcohol (BA) by Sub_C, Sub_E, and Sub_K (Reprinted with permission from ref [132]. Copyright 2015, American Chemical Society).

Not only single phase graphene-based materials (doped one) was simulated, but also graphene-based catalysis over "metal free" composites was also simulated. Xu et al. [133] presented a DFT theoretical calculation result for the origin of enhancing visible-light photocatalytic hydrogen evolution over rGO and g-C_3N_4/rGO composites. The Cambridge Serial Total Energy Package (CASTEP) based on the plane-wave pseudopotential DFT methods was employed. The authors first used a (2 × 2) GR supercell, which matched the g-C_3N_4 unit cell with a small strain less than 2.9%, to simulate the hybrid g-C_3N_4/GR composite. Then the band structure and total DOS was illustrated. The band gap of g-C_3N_4/rGO composite was determined to be 1.7–2.4 eV indicating a direct band gap semiconductor. The interaction between the g-C_3N_4 and rGO sheets was investigated in details. It's found that the oxygen atom in the rGO played a critical role in the composites and negatively charged oxygen atoms served as active sites. All of these beneficial effects brought due to the presence of O atom led to the high H_2 production activity.

Metal/graphene system is another type of simulated catalytic reaction. N-doped carbon support was reported to enhance the stability of Au-based catalysts for acetylene hydrochlorination while the mechanism was not clear. Gu et al. [134] established a big graphene cluster model of $C_{110}H_{28}$ with different nitrogen doping. Three types gold species including Au dimers, Au_2Cl_2 and Au_2Cl_6 were

adsorbed over these carbon supports through theoretical calculations, which aimed on disclosing the reason. The authors carried out the computations using DFT as theoretical basis by Dmol3 code. They first optimized the geometrics of pristine and NG before the Au complex was adsorbed. The doping energy was used to determine the probable location of doped nitrogen atom. Then it's found that the N-doped support GRN-I (the pyridinic N-doped graphene) demonstrated the highest adsorption energies of the Au dimer, Au_2Cl_2 and Au_2Cl_6 among the different supports. Finally, the most stabilized gold species Au_2Cl_6 was selected to further study the effect on the adsorption of reactants C_2H_2 and HCl. With optimized geometry, both adsorbed reactants were activated. Furthermore, Au_2Cl_6/GRN-I could enhance interaction between Au_2Cl_6 and HCl and inhibited the reduction of Au^{3+}, which finally increased the long-term stability of Au-based catalysts.

DFT already shows the great potential on graphene-based catalysis with such short time of its application. Two points are worth mentioning. First, suitable selection of the model system is the most important issue for computational work. It depends on the data from extensive experimental observations. Second, it's highly advised to combine DFT computational results with experimental observations.

4.3. Combination Experimental Observations with Theoretical Computations

Combination experimental observations with theoretical computations to reveal the mechanism of a catalytic reaction is an increasing area and has shown promising results. Here we review two typical examples to illustrate key points and the challenges.

Carbon-based metal free catalysts showed great potentials in electrochemical reactions such as ORR, OER, and HER, while the mechanism is still under debate. N-doped graphene was reported to be a superior catalyst for these reactions. Jia et al. [135] showed that defect graphene had much better performance than N-doped graphene (Figure 11). To explore the mechanism, both experimental observations and theoretical computations approaches were adopted to understand the underlying catalytic mechanisms. The 2D graphene material possessing carbon defects (DG) was synthesized by removing nitrogen from a N-doped graphene under annealing at 1150 °C for 2 h. Several techniques were employed to investigate the structure of DG. XPS confirmed the loss of nitrogen dopant after heat treatment. Increased I_D/I_G ratio compared to NG from Raman spectra indicated a further increase in defects of DG. TEM images supported Raman results, where the holes were clearly observed in the graphene sheet resulting from the removal of nitrogen. High-resolution TEM images further revealed that there were four types of defects, i.e., edge pentagon, 585, 7557, and 5775 defects where the Arabic numerals represent the shape of the defects. Based on these experimental observations, four DFT computational models were developed. In the next step, the authors excluded the possibility of 5775 defect serving as active sites based on the analysis of the frontier molecular orbitals. Then, the minimum energy pathways for the ORR, OER, and HER were calculated. Five defect atomic sites with the highest catalytic activity (5-1, 585-1, 585-3, 7557-1, and 7557-4) were illustrated. Finally, the most active sites for the ORR, OER, and HER were successfully identified by comparing the smallest activation barrier, minimum potential, and lowest free energy respectively, which were consistent with the reported results.

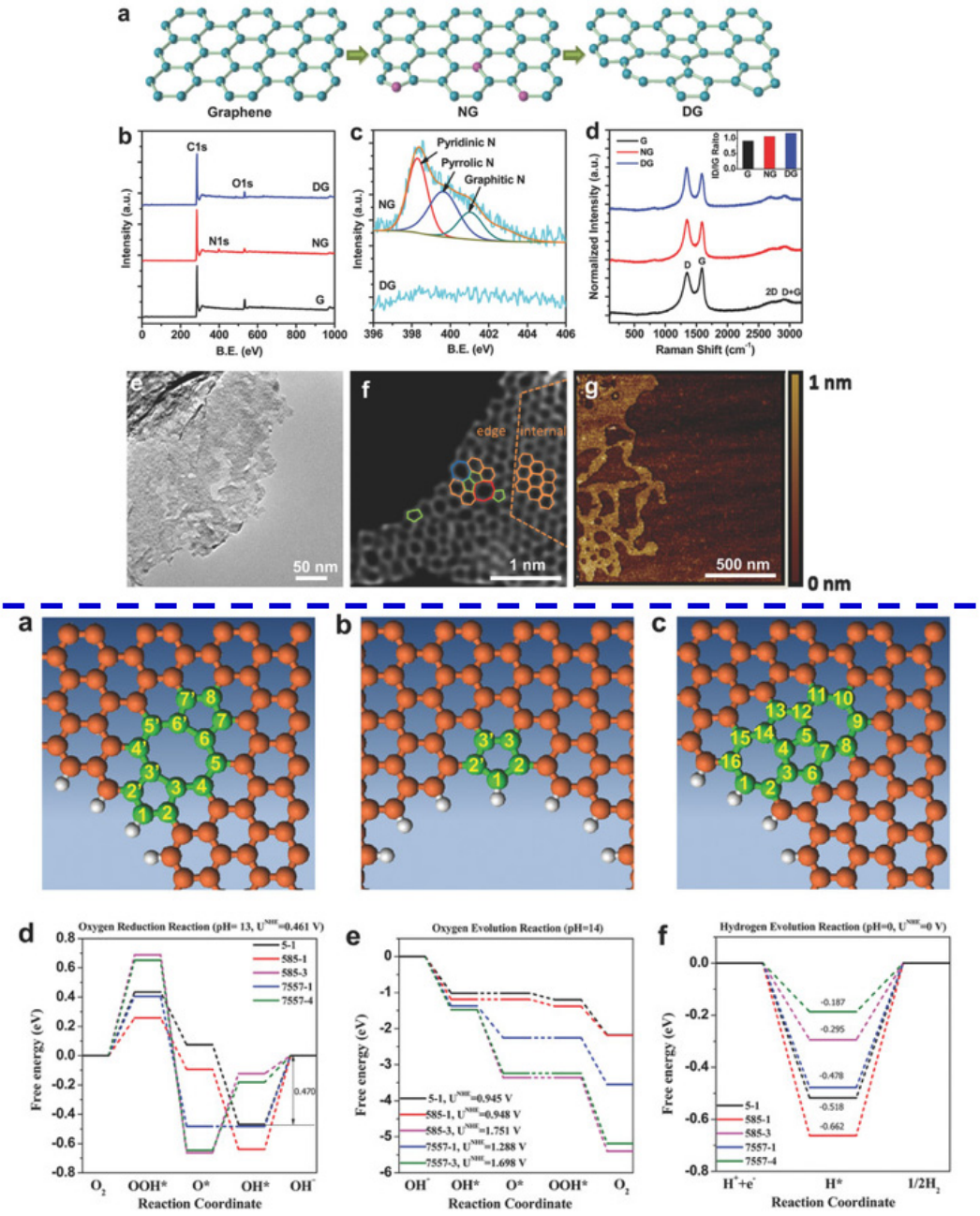

Figure 11. Mechanism exploration of electrochemical reactions (ORR, OER, and HER) over trifunctional defective graphene catalyst by combination of experimental observations and theoretical computations (Reprinted with permission from ref [135]. Copyright 2016, John Wiley & Sons, Inc). Upper figures: Characterizations of the resulting samples: a) Schematic of formation of DG. b) XPS patterns of the pristine graphene, NG, and DG. c) High resolution of N 1s spectra of NG and DG. d) Raman patterns of pristine graphene, NG, and DG. e) The transmission electron microscopy (TEM) image of DG. f) HAADF image of DG. Hexagons, pentagons, heptagons, and octagons were labeled in orange, green, blue, and red, respectively. g) The atomic force microscopy image of DG. Lower figures: DFT calculation results: (a) 5-8-5 defect. (b) Edge pentagon. (c) 7-55-7 defect. (d–f) Schematic energy profiles for the ORR pathway, the OER pathway, and the HER pathway on defective graphene in alkaline/acidic media.

The application of this combination approach was also reported on metal/graphene system for traditional pollutants degradation reaction. Rout et al. [45] synthesized a series of bimetallic Au–Cu alloy nanoparticles (NPs) on reduced graphene oxide support catalysts (Au–Cu/rGO) with different ratios of Au/Cu by a one-step deposition-precipitation method. With optimized formulation, the catalyst demonstrated high activity for reduction of 4-nitrophenol (4-NP) and toxic azo dyes (congo red, methyl orange, and erichrome black T). First, UV-vis measurements indicated the formation of GO and rGO with characteristic peaks at 230 and 270 nm. It was further supported by XRD patterns with detection of the characteristic peak at ~25.3° for rGO. Moreover, the fcc nature was observed for alloy in all samples. FTIR also confirmed the removal of the most oxy-functional groups. TEM indicated the uniform dispersion of Au–Cu nanoparticles without any possible agglomeration. SAED pattern confirmed the fcc feature. XPS further confirmed the removal of functional groups, which led to the generation of defect sites facilitating the efficient deposition of Au–Cu NPs. With DFT, theoretical investigations of mechanism behind the superior catalytic activity were carried out. They used the hybrid exchange-correlation functional B3LYP embedded in Gaussian 09 program. The interaction between the nitro group and catalysts was revealed by investigating the adsorption of the reactant (4-NP) on the different sites of catalyst surface, where calculated adsorption energy and bond length were the two criteria. Based on both experimental and theoretical results, the authors concluded that the unique synergistic effect between rGO support and the highly-dispersed Au–Cu NPs was considered to be the critical factor for the efficient adsorption of 4-NP on the surface, which finally facilitated the reaction.

With combination of experimental observations and theoretical computations, fully understanding the complex catalytic reaction mechanism becomes possible. It's still at the very early stage in graphene-based catalysis. The future development of this approach would be expected.

5. Conclusions

In this article, we comprehensively reviewed the main techniques for graphene-based catalysis covering bulk and surface analysis, chemisorption ability determination, and mechanism investigation. We discussed the applications and challenges of Raman spectroscopy, XPS, FTIR, XRD, XANES and XAFS, AFM, SEM, TEM, HRTEM, UV-vis, XRF, ICP, TGA, BET, STM, and DRIFTS. The application of TPR, CO chemisorption, and NH_3/CO_2-TPD was also briefly introduced. This review provides key information to catalysis community to adopt suitable characterization techniques for their research. These endeavors would help them in deeply and fully understanding these tools, which would be accordingly beneficial their research on graphene-based catalysis.

In spite of the remarkable progress made in graphene-based catalysis with these techniques, it's worth noting that the application of graphene catalysts including their characterizations is only in its infant stage. It should be very careful on choosing suitable tools and interpreting the collected data. Several general issues still exist on characterization of graphene-based catalysis, such as superficial analysis on the collected data, lack of comprehensive understanding with multi-techniques, and difficulty with in situ measurements. In our opinion, the following directions may be helpful and should be paid more attention in the future research. Firstly, the Raman Effect is very weak though it's not true for graphene while it's a big issue for the supported catalytic species. The weak signal would definitely result into low sensitivity, which makes it difficult to measure low concentrations of a substance. Therefore, it's critical to enhance the Raman signals while surface enhanced Raman

spectroscopy (SERS) is a good choice. SERS can significantly enhance the weak Raman signals by several orders of magnitude through chemical (charge transfer) mechanism or electromagnetic mechanism. The former mechanism occurs between adsorbed molecules and the metal surface while the later one is derived from excitation of localized surface Plasmon resonance (LSPR) [36]. SERS has been widely used for characterizing structure and catalytic reaction mechanism over traditional materials while its application on graphene-based catalysts is still rarely reported. It should be developed and will be very useful on deep understanding of active sites on graphene. Secondly, in-situ or operando experiments (IR or Raman), detailed kinetic modelling, and theoretical simulations (DFT) on the interface system are the potential choices in the future study. In-situ or operando experiments can provide "on-site" information of the graphene-based catalyst surface which help to identify the adsorption pattern, intermediates, and fundamental information about the molecular structures of catalysts, leading to revealing the underlying mechanism. Detailed kinetic modelling allowed the description of adsorbed species possible, which is critical for the pathway determination. Theoretical calculations could provide a conceptual framework to help understand how graphene and loaded catalytical species interact, how much the activation energies are as well as how the elementary reaction pathways process. Theoretical simulations (DFT), in most case, is the only available approach to illustrate the complex system related to graphene-based catalysis due to the difficulty existing in the former two methods. Moreover, combining the theoretical computations (DFT) with the experimental observations is a useful and practical approach to fully understand catalytic processes over graphene-based catalysts. Finally, the deep mining over collected data is crucial to fully understand and characterize the graphene-based catalysts. Many skills are required to take full advantage of the data like proficient in using various related software.

Acknowledgements

This work was supported by an ACS-PRF 53582-ND10.

Conflict of Interest

The authors declare no competing financial interest.

References

1. Machado BF, Serp P (2012) Graphene-based materials for catalysis. *Catal Sci Technol* 2: 54–75.
2. Woltornist SJ, Adamson DH (2016) Properties of Pristine Graphene Composites Arising from the Mechanism of Graphene-Stabilized Emulsion Formation. *Ind Eng Chem Res* 55: 6777–6782.
3. Ambrosi A, Chua CK, Latiff NM, et al. (2016) Graphene and its electrochemistry—an update. *Chem Soc Rev* 45: 2458–2493.
4. Novoselov KS, Geim AK, Morozov SV, et al. (2004) Electric field effect in atomically thin carbon films. *Science* 306: 666–669.
5. Hu M, Yao Z, Wang X (2017) Graphene-Based Nanomaterials for Catalysis. *Ind Eng Chem Res* 56: 3477–3502.

6. An D, Yang L, Wang TJ, et al. (2016) Separation performance of graphene oxide membrane in aqueous solution. *Ind Eng Chem Res* 55: 4803–4810.
7. Ding J, Li B, Liu Y, et al. (2015) Fabrication of Fe_3O_4@reduced graphene oxide composite via novel colloid electrostatic self-assembly process for removal of contaminants from water. *J Mater Chem A* 3: 832–839.
8. Kim KL, Lee W, Hwang SK, et al. (2016) Epitaxial Growth of Thin Ferroelectric Polymer Films on Graphene Layer for Fully Transparent and Flexible Nonvolatile Memory. *Nano Lett* 16: 334–340.
9. Khurana G, Misra P, Kumar N, et al. (2014) Tunable Power Switching in Nonvolatile Flexible Memory Devices Based on Graphene Oxide Embedded with ZnO Nanorods. *J Phys Chem C* 118: 21357–21364.
10. Mendoza-Sánchez B, Gogotsi Y (2016) Synthesis of Two-Dimensional Materials for Capacitive Energy Storage. *Adv Mater* 28: 6104–6135.
11. Palaniselvam T, Kashyap V, Bhange SN, et al. (2016) Nanoporous Graphene Enriched with Fe/Co-N Active Sites as a Promising Oxygen Reduction Electrocatalyst for Anion Exchange Membrane Fuel Cells. *Adv Energy Mater* 26: 2150–2162.
12. Wei W, Sun K, Hu YH (2016) Direct conversion of CO_2 to 3D graphene and its excellent performance for dye-sensitized solar cells with 10% efficiency. *J Mater Chem A* 4: 12054–12057.
13. Gao Y, Shiue RJ, Gan X, et al. (2015) Graphene-Boron Nitride Heterostructure Based Electro-Optical Modulator. APS Meeting Abstracts 1: 17005.
14. Furue R, Koveke EP, Sugimoto S, et al. (2017) Arsine gas sensor based on gold-modified reduced graphene oxide. *Sensor Actuat B-Chem* 240: 657–663.
15. Guo R, Zhang S, Xiao M, et al. (2016) Accelerating bioelectric functional development of neural stem cells by graphene coupling: Implications for neural interfacing with conductive materials. *Biomaterials* 106: 193–204.
16. Hu M, Yao Z, Hui KN, et al. (2017) Novel mechanistic view of catalytic ozonation of gaseous toluene by dual-site kinetic modelling. *Chem Eng J* 308: 710–718.
17. Paredes JI, Villar-Rodil S (2016) Biomolecule-assisted exfoliation and dispersion of graphene and other two-dimensional materials: A review of recent progress and applications. *Nanoscale* 8: 15389–15413.
18. Pendashteh A, Palma J, Anderson M, et al. (2017) $NiCoMnO_4$ nanoparticles on N-doped graphene: Highly efficient bifunctional electrocatalyst for oxygen reduction/evolution reactions. *Appl Catal B-Environ* 201: 241–252.
19. Zheng J, Duan X, Lin H, et al. (2016) Silver nanoparticles confined in carbon nanotubes: On the understanding of the confinement effect and promotional catalysis for the selective hydrogenation of dimethyl oxalate. *Nanoscale* 8: 5959–5967.
20. Trapalis A, Todorova N, Giannakopoulou T, et al. (2016) TiO_2/graphene composite photocatalysts for NO_x removal: A comparison of surfactant-stabilized graphene and reduced graphene oxide. *Appl Catal B-Environ* 180: 637–647.
21. Hu M, Hui KS, Hui KN (2014) Role of graphene in MnO_2/graphene composite for catalytic ozonation of gaseous toluene. *Chem Eng J* 254: 237–244.

22. Chavez-Sumarriva I, Van Steenberge PHM, D'Hooge DR (2016) New Insights in the Treatment of Waste Water with Graphene: Dual-Site Adsorption by Sodium Dodecylbenzenesulfonate. *Ind Eng Chem Res* 55: 9387–9396.
23. Zhang N, Yang MQ, Liu S, et al. (2015) Waltzing with the Versatile Platform of Graphene to Synthesize Composite Photocatalysts. *Chem Rev* 115: 10307–10377.
24. Han C, Zhang N, Xu YJ (2016) Structural diversity of graphene materials and their multifarious roles in heterogeneous photocatalysis. *Nano Today* 11: 351–372.
25. Yang MQ, Zhang N, Wang Y, et al. (2017) Metal-free, robust, and regenerable 3D graphene–organics aerogel with high and stable photosensitization efficiency. *J Catal* 346: 21–29.
26. Lu KQ, Zhang N, Han C, et al. (2016) Insight into the Origin of Boosted Photosensitive Efficiency of Graphene from the Cooperative Experiment and Theory Study. *J Phys Chem C* 120: 27091–27103.
27. Quan Q, Lin X, Zhang N, et al. (2017) Graphene and its derivatives as versatile templates for materials synthesis and functional applications. *Nanoscale* 9: 2398–2416.
28. Yang MQ, Zhang N, Pagliaro M, et al. (2014) Artificial photosynthesis over graphene-semiconductor composites. Are we getting better? *Chem Soc Rev* 43: 8240–8254.
29. Zhang Y, Tang ZR, Fu X, et al. (2010) TiO_2–Graphene Nanocomposites for Gas-Phase Photocatalytic Degradation of Volatile Aromatic Pollutant: Is TiO_2–Graphene Truly Different from Other TiO_2–Carbon Composite Materials? *ACS Nano* 4: 7303–7314.
30. Yang MQ, Xu YJ (2013) Selective photoredox using graphene-based composite photocatalysts. *Phys Chem Chem Phys* 15: 19102–19118.
31. Yang MQ, Han C, Zhang N, et al. (2015) Precursor chemistry matters in boosting photoredox activity of graphene/semiconductor composites. *Nanoscale* 7: 18062–18070.
32. Cheng Y, Fan Y, Pei Y, et al. (2015) Graphene-supported metal/metal oxide nanohybrids: synthesis and applications in heterogeneous catalysis. *Catal Sci Technol* 5: 3903–3916.
33. Agnoli S, Favaro M (2016) Doping graphene with boron: A review of synthesis methods, physicochemical characterization, and emerging applications. *J Mater Chem A* 4: 5002–5025.
34. Wang H, Maiyalagan T, Wang X (2012) Review on Recent Progress in Nitrogen-Doped Graphene: Synthesis, Characterization, and Its Potential Applications. *ACS Catal* 2: 781–794.
35. Susi T, Pichler T, Ayala P (2015) X-ray photoelectron spectroscopy of graphitic carbon nanomaterials doped with heteroatoms. *Beilstein J Nanotech* 6: 177–192.
36. Nanda SS, Kim MJ, Yeom KS, et al. (2016) Raman spectrum of graphene with its versatile future perspectives. *TrAC Trends Anal Chem* 80: 125–131.
37. Beams R, Gustavo Cançado L, Novotny L (2015) Raman characterization of defects and dopants in graphene. *J Phys-Condens Mat* 27: 083002.
38. Cao X, Hong T, Yang R, et al. (2016) Insights into the Catalytic Activity of Barium Carbonate for Oxygen Reduction Reaction. *J Phys Chem C* 120: 22895–22902.
39. Hu M, Zhong S (2006) The Structure of TiO_2/Hydroxyapatite and Its Photocatalytic Performance in Degradation of Aldehyde. *Chinese J Catal* 27: 1144.
40. Whelan PR, Jessen BS, Wang R, et al. (2017) Raman spectral indicators of catalyst decoupling for transfer of CVD grown 2D materials. *Carbon* 117: 75–81.
41. Barbon A, Tampieri F (2017) Identification of slow relaxing spin components by pulse EPR techniques in graphene-related materials. *AIMS Mater Sci* 4: 147–157.

42. Deng D, Pan X, Yu L, et al. (2011) Toward N-Doped Graphene via Solvothermal Synthesis. *Chem Mater* 23: 1188–1193.
43. Begliarbekov M, Sul O, Kalliakos S, et al. (2010) Determination of edge purity in bilayer graphene using μ-Raman spectroscopy. *Appl Phys Lett* 97: 031908.
44. Omidvar A, Jaleh B, Nasrollahzadeh M (2017) Preparation of the GO/Pd nanocomposite and its application for the degradation of organic dyes in water. *J Colloid Interf Sci* 496: 44–50.
45. Rout L, Kumar A, Dhaka RS, et al. (2017) Bimetallic Au–Cu alloy nanoparticles on reduced graphene oxide support: Synthesis, catalytic activity and investigation of synergistic effect by DFT analysis. *Appl Catal A-Gen* 538: 107–122.
46. Shahid MM, Rameshkumar P, Basirun WJ, et al. (2017) Cobalt oxide nanocubes interleaved reduced graphene oxide as an efficient electrocatalyst for oxygen reduction reaction in alkaline medium. *Electrochim Acta* 237: 61–68.
47. Ferrari AC, Meyer JC, Scardaci V, et al. (2006) Raman Spectrum of Graphene and Graphene Layers. *Phys Rev Lett* 97: 187401.
48. Rasheed AK, Khalid M, Rashmi W, et al. (2016) Graphene based nanofluids and nanolubricants—Review of recent developments. *Renew Sust Energ Rev* 63: 346–362.
49. Gao N, Fang X (2015) Synthesis and development of graphene-inorganic semiconductor nanocomposites. *Chem Rev* 115: 8294–8343.
50. Tuinstra F, Koenig JL (1970) Raman Spectrum of Graphite. *J Chem Phys* 53: 1126–1130.
51. Oh EJ, Hempelmann R, Nica V, et al. (2017) New catalyst supports prepared by surface modification of graphene- and carbon nanotube structures with nitrogen containing carbon coatings. *J Power Sources* 341: 240–249.
52. Ye T, Durkin DP, Hu M, et al. (2016) Enhancement of Nitrite Reduction Kinetics on Electrospun Pd–Carbon Nanomaterial Catalysts for Water Purification. *ACS Appl Mater Interfaces* 8: 17739–17744.
53. Liu X, Li Z, Zhang B, et al. (2017) Improvement of hydrodeoxygenation stability of nickel phosphide based catalysts by silica modification as structural promoter. *Fuel* 204: 144–151.
54. Qu L, Liu Y, Baek JB, et al. (2010) Nitrogen-doped graphene as efficient metal-free electrocatalyst for oxygen reduction in fuel cells. *ACS Nano* 4: 1321–1326.
55. Liang Y, Li Y, Wang H, et al. (2011) Co_3O_4 nanocrystals on graphene as a synergistic catalyst for oxygen reduction reaction. *Nat Mater* 10: 780–786.
56. Xu X, Yang W, Chen B, et al. (2017) Phosphorus-doped porous graphene nanosheet as metal-free electrocatalyst for triiodide reduction reaction in dye-sensitized solar cell. *Appl Surf Sci* 405: 308–315.
57. He L, Jing L, Luan Y, et al. (2014) Enhanced visible activities of α-Fe_2O_3 by coupling N-doped graphene and mechanism insight. *ACS Catal* 4: 990–998.
58. Yan M, Hua Y, Zhu F, et al. (2017) Constructing nitrogen doped graphene quantum dots-$ZnNb_2O_6$/g-C_3N_4 catalysts for hydrogen production under visible light. *Appl Catal B-Environ* 206: 531–537.
59. Xing T, Zheng Y, Li LH, et al. (2014) Observation of Active Sites for Oxygen Reduction Reaction on Nitrogen-Doped Multilayer Graphene. *ACS Nano* 8: 6856–6862.
60. Hu M, Wang X (2016) Effect of N_3^- species on selective acetylene hydrogenation over Pd/SAC catalysts. *Catal Today* 263: 98–104.

61. Lin C, Wei W, Hu YH (2016) Catalytic behavior of graphene oxide for cement hydration process. *J Phys Chem Solids* 89: 128–133.
62. Yao H, Li F, Lutkenhaus J, et al. (2016) High-performance photocatalyst based on nanosized ZnO-reduced graphene oxide hybrid for removal of Rhodamine B under visible light irradiation. *AIMS Mater Sci* 3: 1410–1425.
63. He Z, Hu M, Wang X (2017) Highly effective hydrodeoxygenation of guaiacol on Pt/TiO_2: Promoter effects. *Catal Today* [In Press].
64. Zhang H, Li W, Jin Y, et al. (2016) Ru–Co(III)–Cu(II)/SAC catalyst for acetylene hydrochlorination. *Appl Catal B-Environ* 189: 56–64.
65. He L, Weniger F, Neumann H, et al. (2016) Synthesis, Characterization, and Application of Metal Nanoparticles Supported on Nitrogen-Doped Carbon: Catalysis beyond Electrochemistry. *Angew Chem Int Ed* 55: 12582–12594.
66. Nguyen DCT, Cho KY, Oh WC (2017) Synthesis of frost-like CuO combined graphene-TiO_2 by self-assembly method and its high photocatalytic performance. *Appl Surf Sci* 412: 252–261.
67. Li F, Yu Z, Shi H, et al. (2017) A Mussel-inspired method to fabricate reduced graphene oxide/g-C_3N_4 composites membranes for catalytic decomposition and oil-in-water emulsion separation. *Chem Eng J* 322: 33–45.
68. Rao CNR, Biswas K, Subrahmanyam KS, et al. (2009) Graphene, the new nanocarbon. *J Mater Chem* 19: 2457–2469.
69. Leng M, Huang X, Xiao W, et al. (2017) Enhanced oxygen evolution reaction by Co–O–C bonds in rationally designed Co_3O_4/graphene nanocomposites. *Nano Energy* 33: 445–452.
70. Annamalai A, Kannan AG, Lee SY, et al. (2015) Role of Graphene Oxide as a Sacrificial Interlayer for Enhanced Photoelectrochemical Water Oxidation of Hematite Nanorods. *J Phys Chem C* 119: 19996–20002.
71. El-Sawy AM, Mosa IM, Su D, et al. (2016) Controlling the Active Sites of Sulfur-Doped Carbon Nanotube–Graphene Nanolobes for Highly Efficient Oxygen Evolution and Reduction Catalysis. *Adv Energy Mater* 6: 1501966–1501977.
72. Yang XD, Zheng Y, Yang J, et al. (2017) Modeling Fe/N/C Catalysts in Monolayer Graphene. *ACS Catal* 7: 139–145.
73. Song X, Shi Q, Wang H, et al. (2017) Preparation of Pd–Fe/graphene catalysts by photocatalytic reduction with enhanced electrochemical oxidation-reduction properties for chlorophenols. *Appl Catal B-Environ* 203: 442–451.
74. Cameron JS, Ashley DS, Andrew JS, et al. (2016) Accurate thickness measurement of graphene. *Nanotechnology* 27: 125704.
75. Wang H, Wei W, Hu YH (2016) Tuning shape of three dimensional graphene sheets. *Catal Today* 274: 99–102.
76. Lu L, Tian H, He J, et al. (2016) Graphene–MnO_2 Hybrid Nanostructure as a New Catalyst for Formaldehyde Oxidation. *J Phys Chem C* 120: 23660–23668.
77. Theerthagiri J, Sudha R, Premnath K, et al. (2017) Growth of iron diselenide nanorods on graphene oxide nanosheets as advanced electrocatalyst for hydrogen evolution reaction. *Int J Hydrogen Energ* 42: 13020–13030.
78. Kashinath L, Namratha K, Byrappa K (2017) Sol-gel assisted hydrothermal synthesis and characterization of hybrid ZnS–RGO nanocomposite for efficient photodegradation of dyes. *J Alloy Compd* 695: 799–809.

79. Wei Z, Chen Y, Wang J, et al. (2016) Cobalt Encapsulated in N-Doped Graphene Layers: An Efficient and Stable Catalyst for Hydrogenation of Quinoline Compounds. *ACS Catal* 6: 5816–5822.
80. Vij V, Tiwari JN, Kim KS (2016) Covalent versus Charge Transfer Modification of Graphene/Carbon-Nanotubes with Vitamin B1: Co/N/S–C Catalyst toward Excellent Oxygen Reduction. *ACS Appl Mater Interfaces* 8: 16045–16052.
81. Hernandez Y, Nicolosi V, Lotya M, et al. (2008) High-yield production of graphene by liquid-phase exfoliation of graphite. *Nat Nanotechnol* 3: 563–568.
82. Reina A, Jia X, Ho J, et al. (2009) Large Area, Few-Layer Graphene Films on Arbitrary Substrates by Chemical Vapor Deposition. *Nano Lett* 9: 30–35.
83. Kuila T, Bose S, Mishra AK, et al. (2012) Chemical functionalization of graphene and its applications. *Prog Mater Sci* 57: 1061–1105.
84. Zhou Y, Bao Q, Tang LAL, et al. (2009) Hydrothermal Dehydration for the "Green" Reduction of Exfoliated Graphene Oxide to Graphene and Demonstration of Tunable Optical Limiting Properties. *Chem Mater* 21: 2950–2956.
85. Hummers Jr WS, Offeman RE (1958) Preparation of graphitic oxide. *J Am Chem Soc* 80: 1339.
86. Kovtyukhova NI (1999) Layer-by-layer assembly of ultrathin composite films from micron-sized graphite oxide sheets and polycations. *Chem Mater* 11: 771–778.
87. Lavin-Lopez MP, Sanchez-Silva L, Valverde JL, et al. (2017) CVD-graphene growth on different polycrystalline transition metals. *AIMS Mater Sci* 4: 194–208.
88. Mo Y, Perez JM, Ye Z, et al. (2016) Effects of light on the resistivity of chemical vapor deposited graphene films. *AIMS Mater Sci* 3: 1426–1435.
89. Hu FM, Kou L, Frauenheim T (2015) Controllable magnetic correlation between two impurities by spin-orbit coupling in graphene. *Sci Rep* 5: 8943.
90. Wang L, Ambrosi A, Pumera M (2013) "Metal-free" catalytic oxygen reduction reaction on heteroatom-doped graphene is caused by trace metal impurities. *Angew Chem Int Ed* 52: 13818–13821.
91. Lupina G, Kitzmann J, Costina I, et al. (2015) Residual Metallic Contamination of Transferred Chemical Vapor Deposited Graphene. *ACS Nano* 9: 4776–4785.
92. Krasheninnikov AV, Nieminen RM (2011) Attractive interaction between transition-metal atom impurities and vacancies in graphene: a first-principles study. *Theor Chem Acc* 129: 625–630.
93. Dasgupta A, Rajukumar LP, Rotella C, et al. (2017) Covalent three-dimensional networks of graphene and carbon nanotubes: synthesis and environmental applications. *Nano Today* 12: 116–135.
94. Wang H, Sun K, Tao F, et al. (2013) 3D honeycomb-like structured graphene and its high efficiency as a counter-electrode catalyst for dye-sensitized solar cells. *Angew Chem Int Ed* 52: 9210–9214.
95. Zheng B, Hermet P, Henrard L (2010) Scanning Tunneling Microscopy Simulations of Nitrogen- and Boron-Doped Graphene and Single-Walled Carbon Nanotubes. *ACS Nano* 4: 4165–4173.
96. Gervasini A, Auroux A (1991) Acidity and basicity of metal oxide surfaces II. Determination by catalytic decomposition of isopropanol. *J Catal* 131: 190–198.
97. Silva CR, Airoldi C (1997) Acid and Base Catalysts in the Hybrid Silica Sol-Gel Process. *J Colloid Interf Sci* 195: 381–387.

98. Glazneva TS, Kotsarenko NS, Paukshtis EA (2008) Surface acidity and basicity of oxide catalysts: From aqueous suspensions to in situ measurements. *Kinet Catal* 49: 859–867.
99. Freese U, Heinrich F, Roessner F (1999) Acylation of aromatic compounds on H-Beta zeolites. *Catal Today* 49: 237–244.
100. Liu SS, Sun KQ, Xu BQ (2014) Specific Selectivity of Au-Catalyzed Oxidation of Glycerol and Other C_3-Polyols in Water without the Presence of a Base. *ACS Catal* 4: 2226–2230.
101. Setoyama T (2006) Acid–base bifunctional catalysis: An industrial viewpoint. *Catal Today* 116: 250–262.
102. Wang H, Deng T, Wang Y, et al. (2013) Graphene oxide as a facile acid catalyst for the one-pot conversion of carbohydrates into 5-ethoxymethylfurfural. *Green Chem* 15: 2379–2383.
103. Xiao C, Goh TW, Qi Z, et al. (2016) Conversion of Levulinic Acid to γ-Valerolactone over Few-Layer Graphene-Supported Ruthenium Catalysts. *ACS Catal* 6: 593–599.
104. Li J, Tang W, Liu G, et al. (2016) Reduced graphene oxide modified platinum catalysts for the oxidation of volatile organic compounds. *Catal Today* 278: 203–208.
105. Wang H, Xiao B, Cheng X, et al. (2015) NiMo catalysts supported on graphene-modified mesoporous TiO_2 toward highly efficient hydrodesulfurization of dibenzothiophene. *Appl Catal A-Gen* 502: 157–165.
106. Bulushev DA, Zacharska M, Lisitsyn AS, et al. (2016) Single Atoms of Pt-Group Metals Stabilized by N-Doped Carbon Nanofibers for Efficient Hydrogen Production from Formic Acid. *ACS Catal* 6: 3442–3451.
107. Zhang L, Liu H, Huang X, et al. (2015) Stabilization of Palladium Nanoparticles on Nanodiamond-Graphene Core-Shell Supports for CO Oxidation. *Angew Chem Int Ed* 54: 15823–15826.
108. Zhang H, Alhamed YA, Al-Zahrani A, et al. (2014) Tuning catalytic performances of cobalt catalysts for clean hydrogen generation via variation of the type of carbon support and catalyst post-treatment temperature. *Int J Hydrogen Energ* 39: 17573–17582.
109. Sun J, Tong X, Liu Z, et al. (2016) Gold-catalyzed selectivity-switchable oxidation of benzyl alcohol in the presence of molecular oxygen. *Catal Commun* 85: 70–74.
110. Upare PP, Lee M, Lee SK, et al. (2016) Ru nanoparticles supported graphene oxide catalyst for hydrogenation of bio-based levulinic acid to cyclic ethers. *Catal Today* 265: 174–183.
111. Xiao X, Sheng Z, Yang L, et al. (2016) Low-temperature selective catalytic reduction of NO_x with NH_3 over a manganese and cerium oxide/graphene composite prepared by a hydrothermal method. *Catal Sci Technol* 6: 1507–1514.
112. Han C, Yang MQ, Weng B, et al. (2014) Improving the photocatalytic activity and anti-photocorrosion of semiconductor ZnO by coupling with versatile carbon. *Phys Chem Chem Phys* 16: 16891–16903.
113. Im K, Nguyen DN, Kim S, et al. (2017) Graphene-Embedded Hydrogel Nanofibers for Detection and Removal of Aqueous-Phase Dyes. *ACS Appl Mater Interfaces* 9: 10768–10776.
114. Huang Y, Tang J, Gai L, et al. (2017) Different approaches for preparing a novel thiol-functionalized graphene oxide/Fe–Mn and its application for aqueous methylmercury removal. *Chem Eng J* 319: 229–239.
115. Li C, Li Z, Cao L, et al. (2016) Graphene Preparation by Phenylmagnesium Bromide and Its Excellent Electrical Conductivity Performance in Graphene/Poly(p-phenylene sulfide) Composites. *Ind Eng Chem Res* 55: 10860–10867.

116. Nie R, Miao M, Du W, et al. (2016) Selective hydrogenation of C=C bond over N-doped reduced graphene oxides supported Pd catalyst. *Appl Catal B-Environ* 180: 607–613.
117. Nørskov JK, Scheffler M, Toulhoat H (2006) Density functional theory in surface science and heterogeneous catalysis. *MRS Bull* 31: 669–674.
118. Norskov JK, Bligaard T, Rossmeisl J, et al. (2009) Towards the computational design of solid catalysts. *Nat Chem* 1: 37–46.
119. Boukhvalov DW (2013) DFT modeling of the covalent functionalization of graphene: From ideal to realistic models. *RSC Adv* 3: 7150–7159.
120. Ferrighi L, Datteo M, Di Valentin C (2014) Boosting graphene reactivity with oxygen by boron doping: Density functional theory modeling of the reaction path. *J Phys Chem C* 118: 223–230.
121. Jiang HR, Zhao TS, Shi L, et al. (2016) First-Principles Study of Nitrogen-, Boron-Doped Graphene and Co-Doped Graphene as the Potential Catalysts in Nonaqueous Li-O_2 Batteries. *J Phys Chem C* 120: 6612–6618.
122. Das R, Dhar N, Bandyopadhyay A, et al. (2016) Size dependent magnetic and optical properties in diamond shaped graphene quantum dots: A DFT study. *J Phys Chem Solids* 99: 34–42.
123. Cantatore V, Panas I (2016) Communication: Towards catalytic nitric oxide reduction via oligomerization on boron doped graphene. *J Chem Phys* 144.
124. Schneider WB, Benedikt U, Auer AA (2013) Interaction of platinum nanoparticles with graphitic carbon structures: A computational study. *ChemPhysChem* 14: 2984–2989.
125. Liu Q, Li ZS, Chen SL (2016) Metal-Embedded Graphene as Potential Counter Electrode for Dye-Sensitized Solar Cell. *Ind Eng Chem Res* 55: 455–462.
126. Chen X, Li F, Zhang N, et al. (2013) Mechanism of oxygen reduction reaction catalyzed by Fe(Co)-N_x/C. *Phys Chem Chem Phys* 15: 19330–19336.
127. Duan X, Ao Z, Zhou L, et al. (2016) Occurrence of radical and nonradical pathways from carbocatalysts for aqueous and nonaqueous catalytic oxidation. *Appl Catal B-Environ* 188: 98–105.
128. Vazquez-Arenas J, Ramos-Sanchez G, Franco AA (2016) A multi-scale model of the oxygen reduction reaction on highly active graphene nanosheets in alkaline conditions. *J Power Sources* 328: 492–502.
129. Kang J, Yu JS, Han B (2016) First-Principles Design of Graphene-Based Active Catalysts for Oxygen Reduction and Evolution Reactions in the Aprotic Li-O_2 Battery. *J Phys Chem Lett* 7: 2803–2808.
130. Gao Y, Tang P, Zhou H, et al. (2016) Graphene Oxide Catalyzed C–H Bond Activation: The Importance of Oxygen Functional Groups for Biaryl Construction. *Angew Chem Int Ed* 55: 3124–3128.
131. Mussell S, Choudhury P (2016) Density Functional Theory Study of Iron Phthalocyanine Porous Layer Deposited on Graphene Substrate: A Pt-Free Electrocatalyst for Hydrogen Fuel Cells. *J Phys Chem C* 120: 5384–5391.
132. Jeyaraj VS, Kamaraj M, Subramanian V (2015) Generalized Reaction Mechanism for the Selective Aerobic Oxidation of Aryl and Alkyl Alcohols over Nitrogen-Doped Graphene. *J Phys Chem C* 119: 26438–26450.
133. Xu L, Huang WQ, Wang LL, et al. (2015) Insights into Enhanced Visible-Light Photocatalytic Hydrogen Evolution of g-C_3N_4 and Highly Reduced Graphene Oxide Composite: The Role of Oxygen. *Chem Mater* 27: 1612–1621.

134. Gu J, Du Q, Han Y, et al. (2014) Nitrogen-doped carbon supports with terminated hydrogen and their effects on active gold species: a density functional study. *Phys Chem Chem Phys* 16: 25498–25507.
135. Jia Y, Zhang L, Du A, et al. (2016) Defect Graphene as a Trifunctional Catalyst for Electrochemical Reactions. *Adv Mater* 28: 9532–9538.

AIMS Press